iScience

CellPress
OPEN ACCESS

Article

TRPC4 deletion elicits behavioral defects in sociability by dysregulating expression of microRNA-138-2

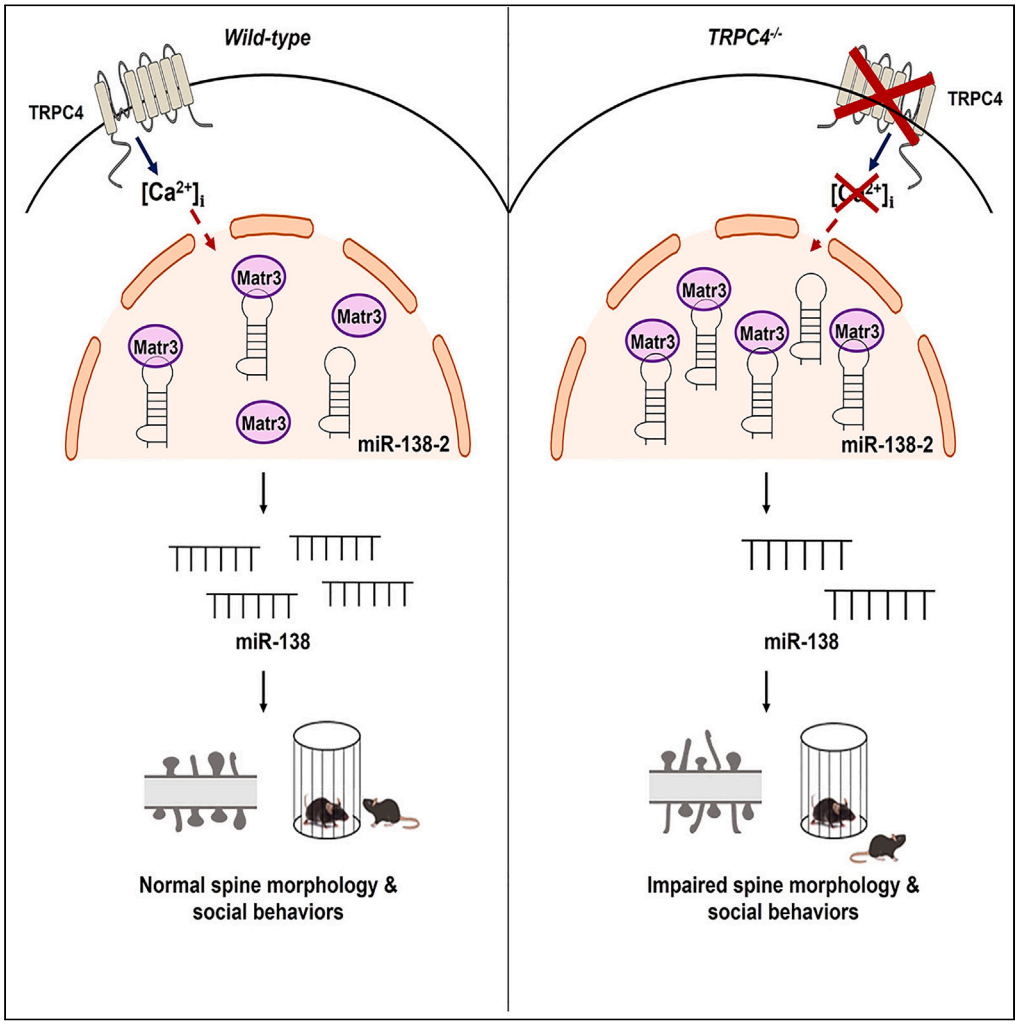

Jee Young Seo, Hye-Ryeong Jo, Seung Hoon Lee, ..., Young In Choi, Sung Jun Jung, Hyeon Son

eurijj@hanyang.ac.kr (S.J.J.)
hyeonson@hanyang.ac.kr (H.S.)

Highlights

Trpc4$^{-/-}$ mice display behavioral defects in sociability and social interaction

MATR3 is downregulated in the hippocampus of *Trpc4*$^{-/-}$ mice

MiR-138 inhibits miR-138-2 processing in the hippocampal neurons in *Trpc4*$^{-/-}$ mice

TRPC4 regulates spine morphology and social behaviors through miR-138

Seo et al., iScience 27, 108617
January 19, 2024
https://doi.org/10.1016/j.isci.2023.108617

iScience

CellPress
OPEN ACCESS

Article

TRPC4 deletion elicits behavioral defects in sociability by dysregulating expression of microRNA-138-2

Jee Young Seo,[1] Hye-Ryeong Jo,[2] Seung Hoon Lee,[2] Do Gyeong Kim,[1] Huiju Lee,[1] Ye Lim Kim,[1] Young In Choi,[3] Sung Jun Jung,[1,3,*] and Hyeon Son[1,4,5,*]

SUMMARY

To investigate whether the defects in transient receptor potential canonical 4 (TRPC4), which is strongly expressed in the hippocampus, are implicated in ASD, we examined the social behaviors of mice in which *Trpc4* was deleted (*Trpc4*$^{-/-}$). *Trpc4*$^{-/-}$ mice displayed the core symptoms of ASD, namely, social disability and repetitive behaviors. In microarray analysis of the hippocampus, microRNA (miR)-138-2, the precursor of miR-138, was upregulated in *Trpc4*$^{-/-}$ mice. We also found that binding of Matrin3 (MATR3), a selective miR-138-2 binding nuclear protein, to miR-138-2 was prominently enhanced, resulting in the downregulation of miR-138 in *Trpc4*$^{-/-}$ mice. Some parameters of the social defects and repetitive behaviors in the *Trpc4*$^{-/-}$ mice were rescued by increased miR-138 levels following miR-138-2 infusion in the hippocampus. Together, these results suggest that *Trpc4* regulates some signaling components that oppose the development of social behavioral deficits through miR-138 and provide a potential therapeutic strategy for ASD.

INTRODUCTION

Autism spectrum disorders (ASDs) are a group of neurodevelopmental disorders characterized by deficits in social communication and interaction, as well as repetitive behaviors and restricted interests.[1,2] Although the molecular mechanisms underlying the development of ASD are not understood, recent research has identified several genes whose deficiency results in synaptic and neural dysfunction and behavioral phenotypes reminiscent of ASD.[3–5] However, it is unclear how genetic and downstream changes converge to mediate ASD behaviors.

Ion channel defects have been implicated in the pathophysiology of ASD. Mutations in genes encoding voltage-gated calcium channels, especially genes encoding the α1 subunit, and abnormalities of potassium channels have been linked to an increased risk of ASD.[6] Transient receptor potential (TRP) channels, which are cation channels that play important roles in sensory signaling, homeostasis, and cellular signaling pathways, may be involved in the development of ASD.[7,8] In particular, defects in TRP canonical 3 (TRPC3) and 6 (TRPC6) are associated with the pathogenesis of ASD in humans.[6] Disruption of TRPC6 has been linked to alterations in neuronal development and the dendritic structure of glutamatergic synapses in non-syndromic autistic individuals.[9] There is also evidence that defects in TRPC3, which is expressed in the Purkinje cells of the cerebellum, affect cognitive functions, motor control, and affective regulation.[10] TRP canonical 4 (TRPC4) and 5 (TRPC5), which have genetically and functionally related subunits, are expressed in the adult rodent and human brains[11] and are thought to play roles in neural plasticity and neurological disease[12,13] through modulation of neuronal growth and Ca^{2+} homeostasis.[14] TRPC4, which is highly expressed in dorsal root ganglia and mediates skin inflammation,[15] is also robustly expressed in the hippocampus of the mouse brain.[11,16] Since the hippocampus has been linked to sociability via social learning and social memory,[17,18] we studied whether defects in hippocampal TRPC4 lead to ASD-like symptoms and, if so, what the underlying mechanisms might be. Here, we show that the social behavioral deficits seen in *Trpc4*$^{-/-}$ mice are accompanied by dysregulated processing of hippocampal miR-138-2. We suggest that hippocampal TRPC4 is a key molecular player in the processes underlying normal sociability via its role in regulating miR-138-dependent synaptic signaling.

RESULTS

Trpc4$^{-/-}$ mice display the typical autistic features of repetitive behaviors and social deficits

To explore whether *Trpc4*$^{-/-}$ mice display behaviors indicative of neuropsychiatric disorders, such as depression and anxiety, we first examined their behaviors in standard assays, including the open field test (OFT), elevated plus maze (EPM), forced swimming test (FST), and grooming.[19] The total grooming time of *Trpc4*$^{-/-}$ mice was twice as long as that of *Trpc4*$^{+/+}$ littermates (Figure 1A). On the other hand,

[1]Graduate School of Biomedical Science and Engineering, Hanyang Biomedical Research Institute, Hanyang University, 222 Wangsimni-ro, Seongdong-gu, Seoul, Korea
[2]Hanyang University Hospital for Rheumatic Diseases, 222 Wangsimni-ro, Seongdong-gu, Seoul, Korea
[3]Department of Physiology, College of Medicine, Hanyang University, 222 Wangsimni-ro, Seongdong-gu, Seoul, Korea
[4]Department of Biochemistry and Molecular Biology, College of Medicine, Hanyang University, 222 Wangsimni-ro, Seongdong-gu, Seoul, Korea
[5]Lead contact
*Correspondence: eurijj@hanyang.ac.kr (S.J.J.), hyeonson@hanyang.ac.kr (H.S.)
https://doi.org/10.1016/j.isci.2023.108617

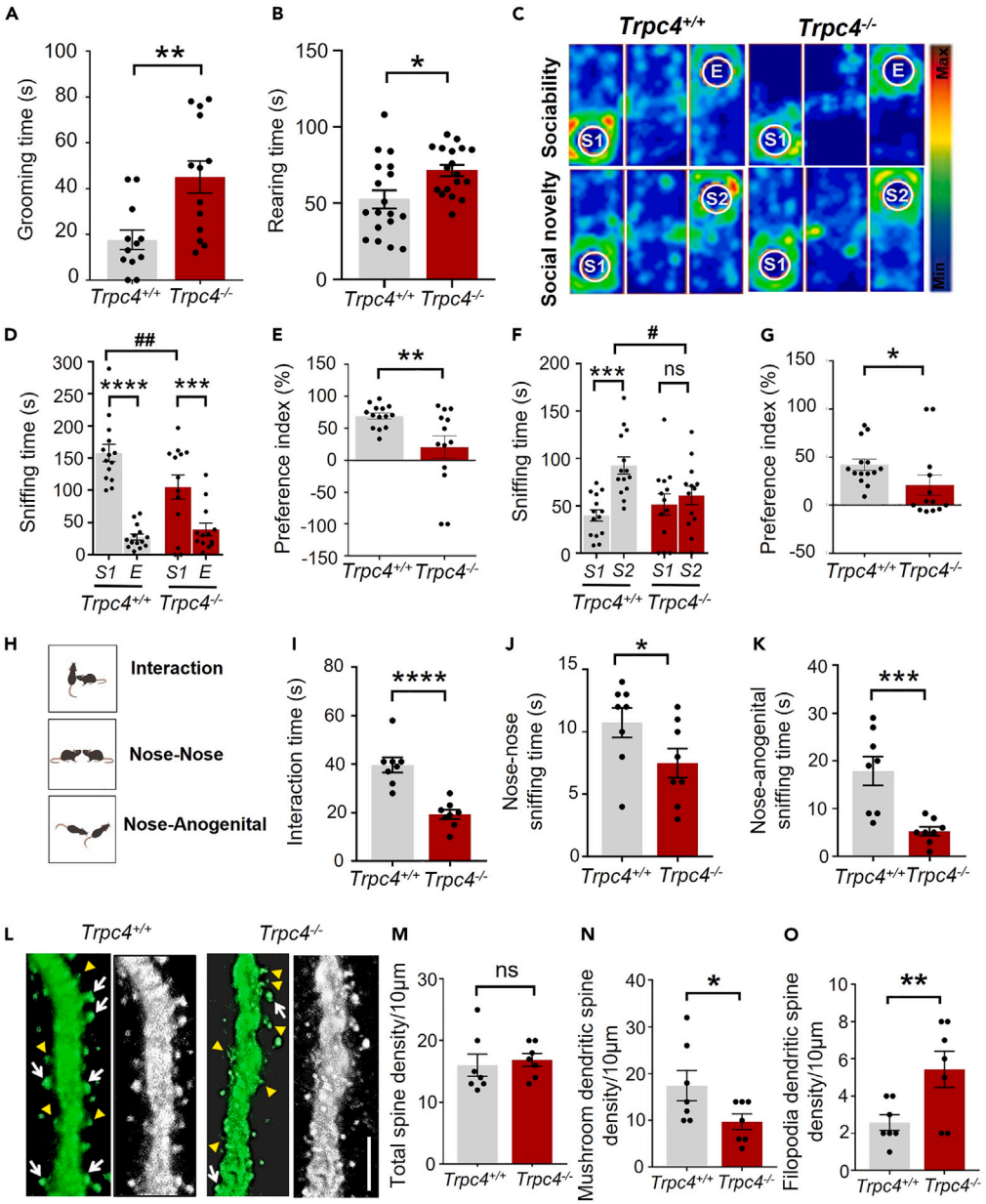

Figure 1. *Trpc4*$^{-/-}$ mice display repetitive behaviors and impaired social behaviors

(A) *Trpc4*$^{-/-}$ mice spent more time self-grooming over a 10-min period than *Trpc4*$^{+/+}$ mice ($p = 0.0017$; $n = 12–13$ per group).

(B) Total time spent on rearing was higher in *Trpc4*$^{-/-}$ mice than *Trpc4*$^{+/+}$ mice ($p = 0.011$, $n = 18$ per each group).

(C) Representative heat maps showing total times and locations during the 10-min social interaction test and social novelty test. Warmer colors indicate more time spent exploring.

(D) In the social interaction test, *Trpc4*$^{+/+}$ and *Trpc4*$^{-/-}$ mice spent significantly more sniffing time with S1 than with the empty cage ($p = 0.0007$). *Trpc4*$^{-/-}$ mice spent significantly less sniffing time with S1 than *Trpc4*$^{+/+}$ mice ($^{\#\#}p = 0.0044$) (Genotype × Chamber interaction $F_{1,50} = 6.642$, $p = 0.013$, $n = 13–14$ per group).

(E) Preference index. *Trpc4*$^{-/-}$ animals had a lower preference for S1 than the controls ($p = 0.0053$, $n = 13–14$ per group).

(F) In the social novelty test, *Trpc4*$^{-/-}$ mice displayed no preference for interaction with the S2 over the S1 mouse ($p = 0.4747$), and spent less time sniffing the S2 than the *Trpc4*$^{+/+}$ mice ($^{\#}p = 0.0174$) (Genotype × Chamber interaction $F_{1,50} = 5.64$, $p = 0.0214$, $n = 13–14$ per group).

(G) The preference index for social novelty recognition was lower in *Trpc4*$^{-/-}$ mice than in *Trpc4*$^{+/+}$ controls ($p = 0.0424$, $n = 13–14$ per group).

(H–K) In the reciprocal sociability test (H), freely interacting dyadic pairs of *Trpc4*$^{+/+}$ - *Trpc4*$^{-/-}$ mice spent less time in reciprocal interaction than *Trpc4*$^{+/+}$ - *Trpc4*$^{+/+}$ pairs (I) they also showed a lower frequency of nose-to-nose interaction (J), and anogenital sniffing (K) (interaction, $p < 0.0001$; nose-nose sniffing, $p = 0.0349$, nose-anogenital, $p = 0.0007$, $n = 8$ per group).

(L) Representative images showing high-magnification z stack projections of apical tuft segments of GFP (+) DG granule cells from lenti-CTL-injected mice.

Figure 1. *Continued*

(M) Total synaptic density was normal in *Trpc4* $^{-/-}$ mice. However, the density of mature dendritic spines of DG granule neurons was reduced ($p = 0.343$). (N) *Trpc4*$^{-/-}$ mice had less mature spines (mushroom) and more immature spines (filopodia) (O) than age-matched *Trpc4*$^{+/+}$ mice. Arrows, mushroom type. Arrowheads, filopodia type (Mushroom: $p = 0.027$; Filopodia: $p = 0.0099$; $n = 7$ per genotype; 10 neurons per mouse; Scale bar: 2.5 μm). Each datum point represents an individual mouse; Data are presented as means ± SEM. *$p < 0.05$, **$p < 0.01$, ***$p < 0.001$, ****$p < 0.0001$. Unpaired *t*-test for (A, B, E, G, I–K, M–O). Two-way ANOVA with Newman-Keuls test (D, F) Multiple comparison post hoc test. Comparisons without an asterisk had $p > 0.05$ and were considered not significant. *ns*, not significant.

total distances traveled were comparable, as assessed in the OFT (Figure S1A), consistent with previous findings that motor function is intact in *Trpc4*$^{-/-}$ mice.[14] In the OFT, *Trpc4*$^{-/-}$ mice also spent more time in the center, thus displaying anxiolytic behavior (Figure S1B), yet times spent in the open and closed arms in the EPM were normal (Figures S1C and S1D). Immobility time in the FST was significantly reduced (Figure S1E), reflecting an antidepressant-like phenotype and consistent with previous results.[14,20] Grooming is a potential correlate of the repetitive behavior observed in ASD.[21] In order to generalize that TRPC4 defects are associated with repetitive behavior, we performed a rearing test, a different repetitive behavior test. *Trpc4*$^{-/-}$ mice spent significantly longer rearing compared to control mice (Figure 1B). We next investigated whether *Trpc4*$^{-/-}$ mice exhibit enhanced motor coordination using the rotarod test. Over the last two trials, the latency to fall from the rotating drum was significantly longer in *Trpc4*$^{-/-}$ mice compared with that of wild-type mice, approaching the 300 s cut-off time (Figure S1F), reflecting enhanced performance of a repetitive motor routine.[22] Together, the data suggest that *Trpc4*$^{-/-}$ mice had excessive repetitive behaviors, including grooming and rearing, as well as anxiolytic behavior along with antidepressant-like behavior in the FST.

We next tested whether *Trpc4*$^{-/-}$ mice display 'dysfunction of social interaction', another core symptom of ASD, using the three-chamber task (Figures 1C and S1G). In this social interaction test, both *Trpc4*$^{+/+}$ and *Trpc4*$^{-/-}$ mice spent more time sniffing around S1 than around the empty cage (Figures 1D and S1H), but the *Trpc4*$^{-/-}$ mice showed significantly less preference for the stranger (S1) than the controls (Figure 1D), as confirmed by the social preference index (Figure 1E). The social novelty recognition test examines the ability to distinguish between a familiar and an unfamiliar mouse; in this test, a second mouse (Novel Mouse, S2) is placed in the empty chamber at the end of a test in which the experimental mouse has been allowed to interact with S1 (Figures 1C and S1G). The *Trpc4*$^{+/+}$ mice spent significantly more time sniffing around S2 than S1, while the *Trpc4*$^{-/-}$ mice did not show this preference despite spending more total time in the chamber containing S2 (Figures 1F and S1I). Thus, the preference behavior of the *Trpc4*$^{-/-}$ mice was significantly lower than that of the wild-type mice, pointing to perturbed recognition of social novelty (Figure 1G). Together, these results suggest that *Trpc4*$^{-/-}$ mice exhibit impaired sociability.

Next, we applied the reciprocal social interaction test for sociability (Figure 1H). *Trpc4*$^{-/-}$ mice exhibited a significant reduction in contact time (Figure 1I), as well as in the number of successive nose-to-nose (Figure 1J), and nose-to-anogenital sniffing interactions with a freely moving novel mouse (Figure 1K). To rule out general olfactory impairment, we examined the time required to find a buried food pellet and observed no difference between control and *Trpc4*$^{-/-}$ mice (Figure S2A). In the novel object recognition (NOR) task, there were no significant differences in discrimination index between the control and the *Trpc4*$^{-/-}$ mice (Figure S2B), indicating that the impairment of sociability is not due to an inability to recognize familiarity. Taken together, our results indicate that *Trpc4*$^{-/-}$ mice displayed the core symptoms of ASD, including excessive repetitive behaviors and reduced social interaction, as well as impaired social novelty recognition, without displaying the confounding comorbidities of heightened anxiety.

Since TRPC4 knockdown is associated with increased dendritic growth,[23] we investigated whether TRPC4 deficiency increased dendritic growth in the dentate gyrus (DG) of the hippocampus. We inspected the morphology of dendritic spines in lenti-GFP-labeled granule neurons and found that the granule neurons in *Trpc4*$^{-/-}$ mice had a variety of spines, including mushroom, stubby, and filopodia spines, like their *Trpc4*$^{+/+}$ littermates (Figure 1L) and the mean spine density was unchanged (Figure 1M). Interestingly, the numbers of mushroom-like spines were significantly reduced in the *Trpc4*$^{-/-}$ mice (Figure 1N), while filopodia-type and thin spines were more numerous (Figure 1O). Since increases in filopodia and elongated dendritic spines are associated with autism in fragile X syndrome,[24] our results suggest autism-like behaviors are linked to impaired spine morphology in the hippocampus of *Trpc4*$^{-/-}$ mice.

MiR-138-2 signaling is dysregulated in the *Trpc4*$^{-/-}$ hippocampus

To investigate any effects on gene expression in *Trpc4*$^{-/-}$ mice, we performed a genome-wide microarray analysis of hippocampal tissues at 8 weeks (Figure S3A and Table S1), a time when hippocampal expression of TRPC4 is at its peak in the wild-type.[11] The hippocampus is required for social recognition memory, due to its role in recognition and spatial reasoning,[25,26] thus raising the possibility that a lack of TRPC4 in the hippocampus is responsible for modifying social behavior. In the microarray analysis, 142 of the 35240 assayed probe sets (71 up-regulated and 71 down-regulated) were found to be differentially expressed in the hippocampal tissue of *Trpc4*$^{-/-}$ mice (Figure 2A, NCBI accession #GSE220926). GO analysis revealed that 18 of these differentially expressed genes (DEGs) were associated with GO terms relevant to nervous system development and function (Table S2); others were associated with biological processes and cellular components. TRPC4 expression itself was one of the 10 most differentially expressed genes when the criteria were further strengthened (cut-off $p < 0.01$ and intensity > 6.0) (Figure 2B; Table S3).

To obtain first-hand insight into any involvement of miR-138-2 in the behavioral deficits of *Trpc4*$^{-/-}$ mice, we examined the expression of mature miR-138-5p (hereinafter referred to as miR-138), and precursor (pre-) miR-138-2. Using qPCR, we observed an increased level of miR-138-2 in the hippocampus of *Trpc4*$^{-/-}$ mice, in agreement with the microarray results (Figure 2C). Since miR-138-2 is the primary source of

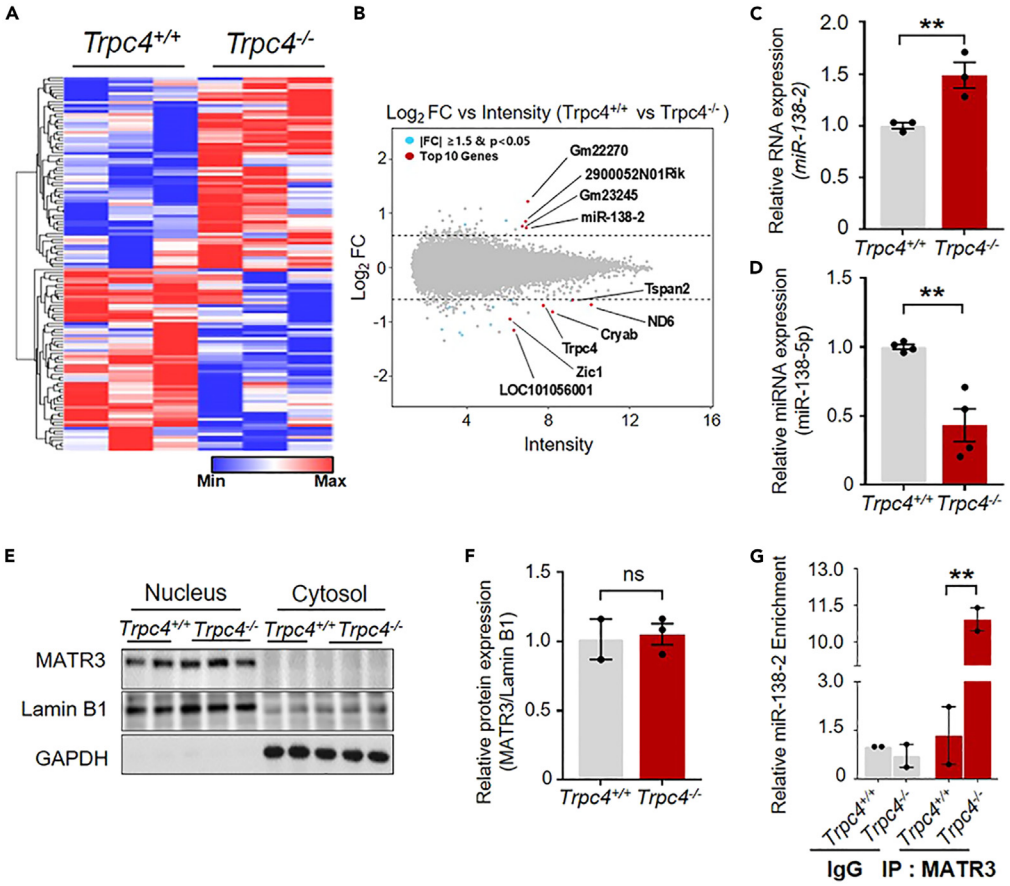

Figure 2. Microarray analysis of hippocampal brain tissue of *Trpc4*$^{-/-}$ mice

RNA samples of hippocampal brain tissue from three pairs of *Trpc4*$^{-/-}$ mice and *Trpc4*$^{+/+}$ littermates were analyzed on Affymetrix Mouse Gene 2.0 ST arrays.

(A) Hierarchical clustering shows the differential expression of genes in *Trpc4*$^{-/-}$ and *Trpc4*$^{+/+}$ hippocampi. (See Table S2 for all fold changes in expression of marker genes and statistics). Rows indicate individual mRNA expression values, and columns indicate different treatment groups. Red and blue indicate high and low expression, respectively.

(B) MA plot of the normalized microarray data. The normalized values are depicted as $\log_2$-fold changes of spot intensity ($M = \log_2(R/G)$) plotted against average log intensities ($A = \log_2 \sqrt{RG}$) (R, Cy5; G, Cy3). The dotted line represents a fold change of 1.5. Red dots indicate the 10 most differentially expressed genes (DEGs) with p values < 0.01 and |fold change| > 1.5.

(C) qRT-PCR validation of the dysregulated expression of miR-138-2 in the hippocampus of *Trpc4*$^{-/-}$ mice. Bar diagram showing the upregulated expression of miR-138-2 in *Trpc4*$^{-/-}$ mice compared to *Trpc4*$^{+/+}$ mice ($p = 0.009$, $n = 3$ per group). Quantitative data of miR-138-2 were normalized with the level of GAPDH.

(D) qRT-PCR of miR-138. Endogenous miR-138 is downregulated in the hippocampus of *Trpc4*$^{-/-}$mice. Mature miR-138-5p expression was normalized to *U6* snRNA ($p = 0.002$, $n = 4$ per group).

(E) The localization of MATR3 categorized as nuclear or cytoplasmic in *Trpc4*$^{+/+}$ and *Trpc4*$^{-/-}$ mice.

(F) Quantitative analysis of nuclear MATR3 immunoreactivity.

(G) RIP analysis of miR-138-2 associated with hippocampal MATR3 in *Trpc4*$^{+/+}$ and *Trpc4*$^{-/-}$ mice. Results were obtained by enrichment analysis of miR-138-2 in anti-MATR3 IPs and compared with IgG-IP controls by qRT-PCR. Fold enrichments of the immunoprecipitated miR-138-2 were calculated as $2^{(\Delta\Delta Ct\ [RIP/background])}$ and are indicated as ratios of miR-138-2 to the IgG-IP controls in *Trpc4*$^{+/+}$ mice (*Trpc4*$^{+/+}$ vs. *Trpc4*$^{-/-}$, $p = 0.005$, $n = 2$ per group). Data are presented as mean ± SEM. **$p < 0.01$. Unpaired *t*-tests. Comparisons with no asterisk had $p > 0.05$ and were considered not significant. *ns*, not significant.

mature-miR-138 in rodent hippocampal neurons,[27] we investigated levels of mature-miR-138. These were halved in *Trpc4*$^{-/-}$ mice (Figure 2D). MiR-29a, an additional miRNA showing a non-significant decrease in *Trpc4*$^{-/-}$ mice by microarray analysis (Table S4), yielded a similar result by qPCR, supporting the use of $p < 0.05$ as the significance cut-off for microarray analysis. Expression of miR-138-2 in the *Trpc4*$^{-/-}$ cells was increased relative to control, while that of miR-138 was reduced, indicating that the processing of miR-138-2 and biogenesis of miR-138 are altered in the absence of TRPC4.

In an effort to explain the lowered miR-138 level in *Trpc4*$^{-/-}$ mice, we investigated whether abnormally high levels of miR-138-2 were retained in the nucleus by MATR3, a selective miR-138-2 binding nuclear protein, which would lead to reduced miR-138 cleavage in the cytoplasm. Western blots showed similar levels of nuclear localization of MATR3 in *Trpc4*$^{+/+}$ and *Trpc4*$^{-/-}$ mice (Figures 2E and 2F). We

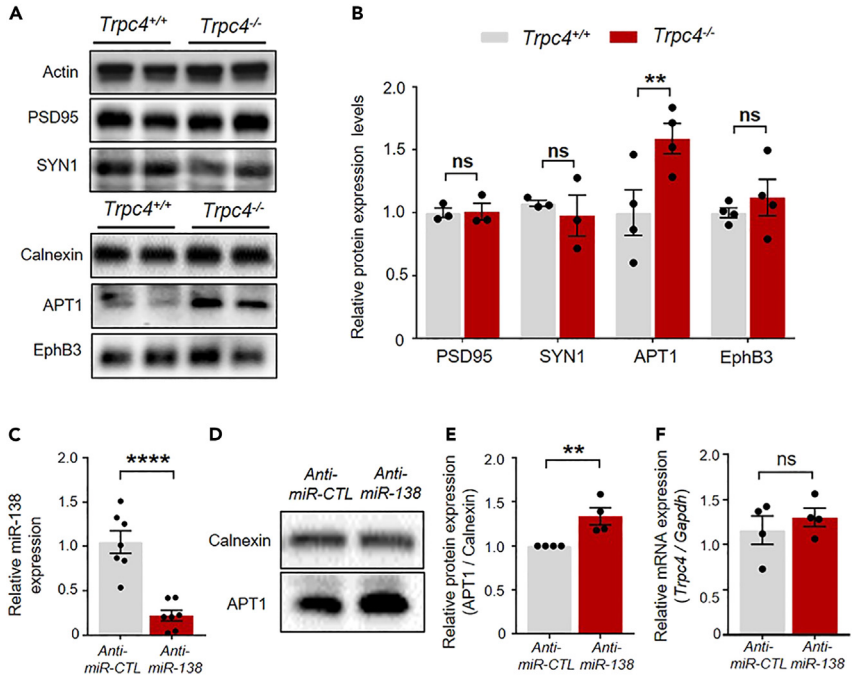

Figure 3. Inhibition of miR-138 affects APT1 expression in *Trpc4*$^{-/-}$ mice

(A and B) Representative immunoblots and quantitative data of synaptic function-related proteins in the hippocampus. The level of APT1 was higher in the *Trpc4*$^{-/-}$ hippocampus than in that of *Trpc4*$^{+/+}$ mice. However, the levels of PSD95, SYN1, and EphB3 were not significantly changed in *Trpc4*$^{-/-}$ mice.

(C) LNA-anti-miR-138 (anti-miR-138, 50 nM) was introduced into cultured hippocampal neurons and DIV13, and it reduced the endogenous level of miR-138 ($p < 0.001$, $n = 7$). The expression of miR-138 was analyzed by qRT-PCR, and is expressed as fold changes relative to those in the anti-miR-CTL.

(D and E) Representative immunoblots and quantitative data for APT1 normalized with the level of calnexin. Levels of APT1 are shown as fold changes relative to those of the anti-miR-CTL ($p < 0.01$, $n = 4$).

(F) The expression of *Trpc4* mRNA measured by qRT-PCR was not changed by anti-miR-138. Expressions are indicated as fold changes relative to anti-miR-CTL. Each data point represents an individual sample; Data are means ± SEM. $^{**}p < 0.01$. $^{***}p < 0.001$. Unpaired *t*-tests. *ns*, not significant.

then used a candidate approach with MATR3 to examine the binding of MATR3 to miR-138-2 in hippocampal lysates by RNA immunoprecipitation and found that levels of miR-138-2 obtained by MATR3 pulldown were much higher in the *Trpc4*$^{-/-}$ mice (Figure 2G). Evidently, the binding of nuclear miR-138-2 to MATR3 is elevated, restricting the cytoplasmic processing of miR-138-2 and reducing levels of mature miR-138.

MiR-138 is known to affect synapse formation in the hippocampus, particularly synaptic spine formation, by negatively regulating the expression of APT1 and EphB3.[28] Therefore, we investigated if the lowered level of miR-138 changed the make-up of the spines in *Trpc4*$^{-/-}$ mice. We found that expression of APT1 was significantly elevated in *Trpc4*$^{-/-}$ mice, whereas we did not observe an increase in levels of PSD95 or SYN1, whose expression is independent of miR-138. Consistent with the negative regulation of APT1 by miR-138 proposed previously[28] and the downregulation of miR-138 in *Trpc4*$^{-/-}$ mice observed in the present study, expression of APT1 was elevated in the hippocampus of *Trpc4*$^{-/-}$ mice (Figures 3A and 3B). In contrast, there were no differences in the levels of miR-138 and APT1 in the prefrontal cortex of *Trpc4*$^{+/+}$ and *Trpc4*$^{-/-}$ mice (Figure S4), which suggests that TRPC4 deletion may only affect levels of miR-138 in specific brain regions. Consistent with the inhibition of APT1 expression by miR-138, inhibition of miR-138 function with an LNA-anti-miR-138 (anti-miR-138) led to significant upregulation of APT1 in the mouse hippocampal neurons (Figures 3C–3E). The antibody had no effect on the expression of *Trpc4* mRNA measured by qPCR, suggesting that miR-138 may not regulate TRPC4 expression (Figure 3F).

The proposed role of TRPC4 deficiency-mediated dysregulation in miR-138 expression led us to examine whether the pharmacological blockade of TRPC4 could also alter the level of miR-138 and social behaviors. Mice were injected with saline or 20 mg/kg M084,[20] a specific inhibitor of TRPC4/5[29] previously shown to produce antidepressant-like and anxiolytic effects in mice upon single administration.[20] Intraperitoneal injection of M084 reduced hippocampal miR-138 2 h later (Figure 4A). Then, we examined the binding of MATR3 to miR-138-2 by RNA immunoprecipitation in hippocampal lysates obtained from saline and M084-treated mice and found that levels of miR-138-2 obtained by MATR3 pulldown were higher in the M084-treated mice than in the saline-treated mice (Figure 4B), consistent with the idea that disruption of TRPC4 signaling is associated with reduced expression of miR-138, and that miR-138 is downstream of TRPC4. M084-treated mice increased APT1 expression compared with saline mice (Figures 4C and 4D). In terms of sociability, although the M084-treated mice showed a reduced preference for S1 (Figure 4E), this effect did not reach statistical significance (Figure 4F). However, M084 did significantly reduce the preference for S2 over S1 in the social novelty recognition test (Figures 4G and 4H).

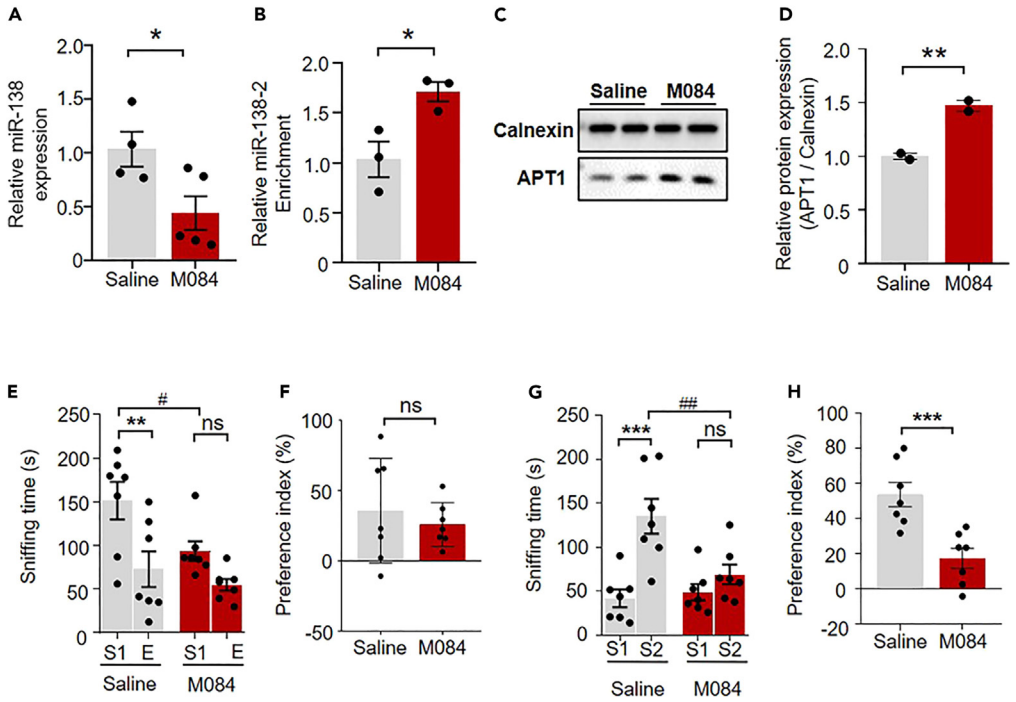

Figure 4. TRPC4 antagonist M084 downregulates hippocampal miR-138 and partially
mimics the behavioral deficits in sociability of *Trpc4*$^{-/-}$ mice.

(A) M084 reduced hippocampal mature miR-138. M084 (20 mg/kg) was injected i.p and 2 h later levels of miR-138 were measured by qRT-PCR in the hippocampus. Expression levels were calculated relative to injection of control *U6* snRNA and are shown as treated/control levels of miR-138 (miR-138-2: $p = 0.338$; miR-138: $p = 0.017$, $n = 4$–5 per group).

(B) RIP analysis of miR-138-2 associated with MATR3 from the hippocampus in Saline and M084 treated mice. Enrichment analysis of miR-138-2 in anti-MATR3 IP compared to IgG-IP controls by qRT-PCR (saline vs. M084, $p = 0.014$, $n = 3$ per group).

(C) Representative immunoblots showing APT1 protein in the hippocampus in saline and M084 treated mice.

(D) Quantification of the APT1 protein levels shown in (C) (saline vs. M084, $p = 0.007$, $n = 2$ per group).

(E) Control mice injected with saline, but not those treated with M084, displayed a preference for S1 over empty cage (**$p = 0.0023$; $^{\#}p = 0.0193$, $n = 7$ per group).

(F) The preference index for S1 did not differ between treated and control mice ($p = 0.266$, $n = 7$ per group).

(G) Mice injected with M084 spent significantly less time interacting with S2 than saline-treated controls ($^{\#\#}p = 0.0018$, $n = 7$ per group).

(H) Preference index showed a decrease in preference for S2 in mice treated with M084 compared with saline-treated controls ($p = 0.0008$, $n = 7$ per group). Each data point represents an individual mouse. Data are means ± SEM. *$p < 0.05$, **$p < 0.01$, ***$p < 0.001$. Unpaired *t*-tests for (A-D, F, H).

Together, these results suggest that miR-138-2 processing is reduced in *Trpc4*$^{-/-}$ mice and leads to downregulation of miR-138 and upregulation of APT1. These findings encouraged us to further examine the role of hippocampal TRPC4 in controlling social behaviors via miR-138.

MiR-138 overexpression rescues the defects in sociability of *Trpc4*$^{-/-}$ mice

Having implicated the reduction in hippocampal miR-138 in the behavioral deficits in *Trpc4*$^{-/-}$ mice, we next sought to determine whether overexpression of miR-138 could rescue the behavioral defects of the *Trpc4*$^{-/-}$ mice. We stereotaxically injected lenti-miR-138-2 or scrambled lenti-CTL into DG coordinates (bilaterally in both hippocampi) and monitored behaviors three weeks later (Figure 5A). Stable viral expression was observed in the hippocampal DG (Figure 5B). However, we detected no significant difference in mature miR-138 levels between *Trpc4*$^{+/+}$ mice infused with lenti-CTL and lenti-miR-138-2 (Figure 5C), in partial agreement with earlier studies suggesting a disparity between precursor and mature miR-138 levels in mouse neurons.[27,30] One possible explanation for this lack of effect of lenti-miR-138-2 in the *Trpc4*$^{+/+}$ mice is that they may already have maximal levels of miR-138. In contrast, there was a significant increase of miR-138 in the hippocampal DG of the *Trpc4*$^{-/-}$ mice infused with lenti-miR-138-2 (Figure 5C), and APT1 levels were significantly reduced (Figures 5D and 5E).

Locomotor activities and levels of anxiety in the OFT and EPM, respectively, were similar in control and mutant mice (Figures S5A–S5C), indicating that the effects of overexpressing miR-138-2 were not attributable to changes in locomotion or sedation. Lenti-miR-138-2 significantly decreased time spent grooming in the *Trpc4*$^{-/-}$ but not in the *Trpc4*$^{+/+}$ mice (Figure 5F). Similarly, miR-138-2 overexpression only reduced time spent on rearing in the *Trpc4*$^{-/-}$ mice, although there was no interaction between genotype and activity (Figure 5G). In the NOR test, both sets of mice differentiated between familiar versus novel objects regardless of miR-138 level (Figure S5D), and

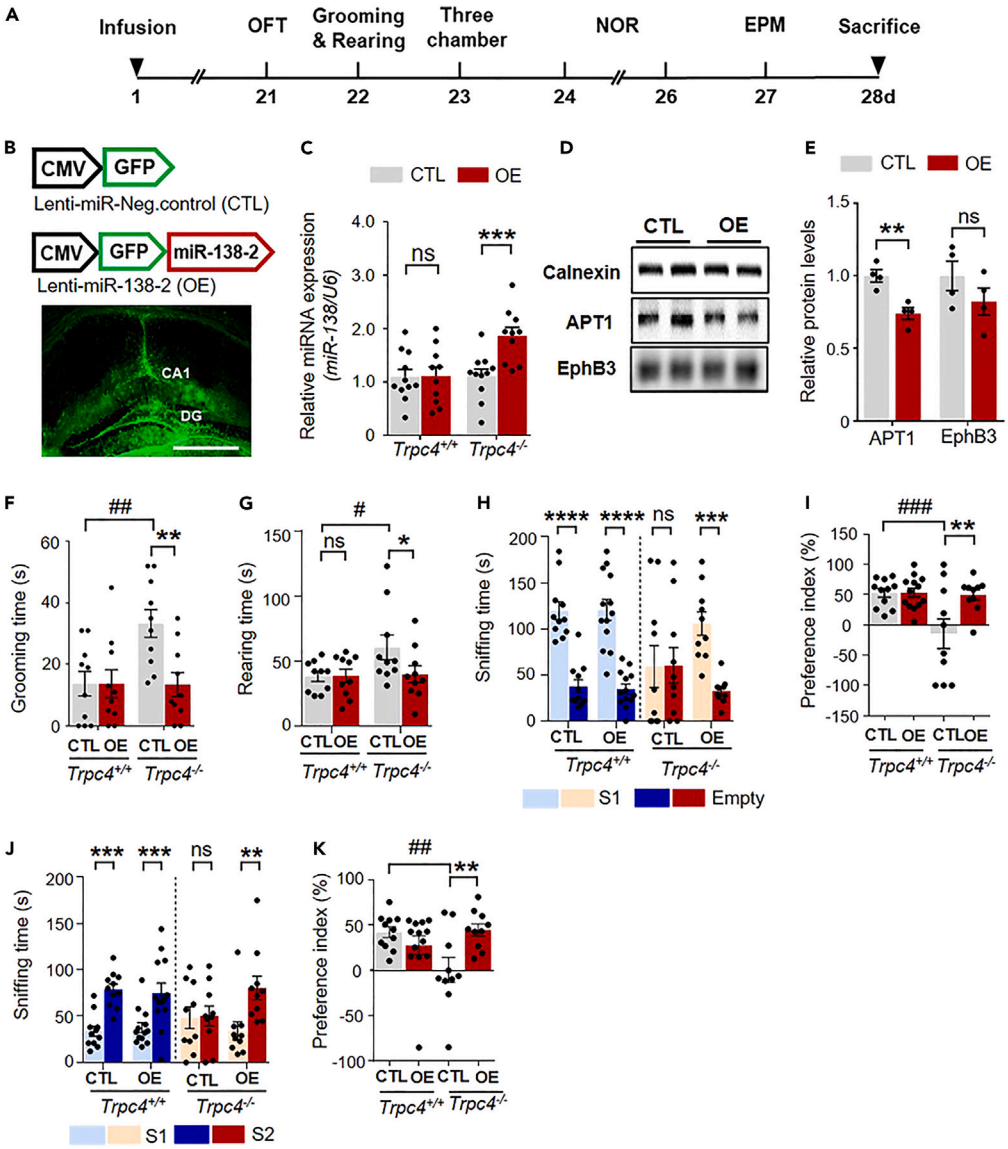

Figure 5. Behavioral phenotypes caused by *Trpc4* deficiency are rescued by targeted overexpression of miR-138 in the hippocampal DG

(A) Timeline of the experimental procedure.

(B) Schematic illustration of control viral vectors (CTL) lenti-miR-138-2 (OE), and GFP immunostaining confirming localization of lentivirus infusion in the hippocampal DG.

(C) Levels of miR-138 in the DG were upregulated in $Trpc4^{-/-}$, but not in $Trpc4^{+/+}$, mice infused with lenti-miR-138-2 compared with lenti-CTL, respectively ($Trpc4^{+/+}$: $p = 0.4693$; $Trpc4^{-/-}$: $p = 0.0008$, $n = 10–11$ per group).

(D) Representative immunoblots of APT1 and EphB3 in hippocampal DG lysates.

(E) APT1 levels were reduced in mice expressing miR-138, while the levels of EphB3 were not significantly affected (APT1: $p = 0.0023$; EphB3: $p = 0.125$ $n = 4$ per group).

(F) Grooming behavior. Lent-miR-138-2 did not significantly change grooming behavior in $Trpc4^{+/+}$ mice. However, it reduced time spent grooming in $Trpc4^{-/-}$ mice ($^{\#\#}p = 0.0022$). (Genotype x Overexpression $F_{1,36} = 5.443$, $p = 0.0254$, $n = 10$ per group).

(G) $Trpc4^{+/+}$ mice infused with lenti-CTL and lenti-miR-138-2 displayed no significant difference in the rearing test ($Trpc4^{+/+}$ mice, lenti-CTL vs. lenti-miR-138-2, $p = 0.948$). Lenti-miR-138-2 reduced time on rearing in $Trpc4^{-/-}$ mice compared with those infused with lenti-CTL, recovered to levels in $Trpc4^{+/+}$ mice ($Trpc4^{-/-}$, lenti-CTL vs. lenti-miR-138-2, $p = 0.032$; Genotype x overexpression $F_{1,36} = 2.65$, $p = 0.1123$, $n = 9–10$ per group).

(H) Social interaction test. $Trpc4^{+/+}$ mice infused with lenti-CTL and lenti-miR-138-2 showed a significant preference for S1 over the empty cage (lenti-CTL & lenti-miR-138-2, S1 vs. E, $p < 0.0001$, respectively), whereas $Trpc4^{-/-}$ mice infused with lenti-CTL showed no preference for S1 relative to empty cage ($p = 0.9485$). However, $Trpc4^{-/-}$ mice, when infused with lenti-miR-138-2, spent more time sniffing with S1 than in an empty cage (Genotype x Overexpression $F_{3,80} = 2.8$, $p = 0.0452$, $n = 10–13$ per group).

Figure 5. *Continued*

(I) Preference index. *Trpc4*$^{-/-}$ mice infused with lenti-CTL showed less social interaction than *Trpc4*$^{+/+}$ controls ($^{\#\#}p = 0.0009$). However, when *Trpc4*$^{-/-}$ mice were infused with lenti-miR-138-2 their preference index increased to the level of *Trpc4*$^{+/+}$ controls ($p = 0.0019$). (Genotype x Overexpression $F_{1,40} = 5.928$, $p = 0.0195$, $n = 10–13$ per group).

(J) In the social novelty test, *Trpc4*$^{-/-}$ mice infused with lenti-CTL displayed no significant preference for the S2 over the S1 ($p = 0.8896$). However, when infused with lenti-miR-138-2 they had a preference for the S2 over the S1 ($p = 0.001$). (Genotype × Overexpression interaction $F_{3,80} = 1.966$, $p = 0.1257$, $n = 10–13$ per group).

(K) The preference index for social novelty was significantly lower in *Trpc4*$^{-/-}$ mice infused with lenti-CTL than in *Trpc4*$^{+/+}$ controls ($p = 0.0037$), but it increased after lenti-miR-138-2 infusion in the *Trpc4*$^{-/-}$ mice ($p = 0.0292$). (Genotype × Overexpression interaction $F_{1,40} = 9.097$, $p = 0.0044$, $n = 10–13$ per group). Each data point represents an individual mouse; Data are means ± SEM. $^{*}p < 0.05$, $^{**}p < 0.01$, $^{***}p < 0.001$, $^{****}p < 0.0001$; Unpaired *t*-tests for (C, E). Two-way ANOVA with Newman-Keuls multiple comparison post hoc test (F-K). *ns*, not significant. Source data were provided as a source data file. Scale bar: 50 μm.

lenti-miR-138-2 had no effect on social interaction and novelty recognition behaviors in *Trpc4*$^{+/+}$ control mice (Figures 5H and 5J), whereas it increased the preference of *Trpc4*$^{-/-}$ mice for S1 versus empty cage (Figure 5H), implying some recovery of social interaction (Figure 5I). *Trpc4*$^{-/-}$ mice infused with lenti-miR-138-2 also exhibited an increased preference for S2 over S1 (Figure 5J), and the preference index revealed that the effects of miR-138 overexpression were significantly greater in the *Trpc4*$^{-/-}$ mice, implying restoration of social novelty recognition in the former (Figure 5K). These data suggest that the behavioral changes could be prevented, at least in part, by overexpressing miR-138 in the hippocampus, consistent with our evidence that miR-138 plays a critical role in the control of social behaviors.

DISCUSSION

We have demonstrated that ablation of TRPC4 causes significant impairment of sociability and response to social novelty and increases repetitive behaviors. ASD is diagnosed based on dysfunction in two core symptom domains: 'social communication/interaction' and 'restricted and repetitive patterns of behavior, interests, or activities (RRB)'.[31] Thus, the behavioral traits of *Trpc4*$^{-/-}$ mice are ASD-like, with prominent RRB domain symptoms, featuring repetitive grooming behaviors accompanied by a decreased preference for social interaction. We further showed that TRPC4 deficiency dysregulates miR-138-2 processing, resulting in a decrease in miR-138, and altered hippocampal dendritic spine morphogenesis, pointing to a hitherto unrecognized complexity of miR-138 function in preventing autistic-like behaviors in mice. The present study identifies TRPC4 as a likely determinant of social behaviors and provides the first hint that TRPC4 might play a role in the processes that are compromised in ASD, in conjunction with miR-138. Given that ASD is diagnosed on the basis of an aberrant behavioral phenotype rather than a biochemical or physiological biomarker,[32] *Trpc4*$^{-/-}$ mice may be a suitable model for investigating the neural mechanisms that are affected in ASD.

Other studies have shown that TRPC4 knockdown increases neurite extension,[33] and TRPC5 activation inhibits dendritic growth in rat neurons.[34] Behaviorally, TRPC4 channel inhibition has been linked to anxiolytic-like behavior and anti-depressive action in mice.[14,20,35] Although it is generally assumed that ASD is linked to increased anxiety, some genetic models, like vaccinia-related kinase 3 knockout (*Vrk3*$^{-/-}$), methyl CpG binding protein 2 knockout (*Mecp2*$^{-/-}$) and cyclin-dependent kinase-like 5 knockout (*Cdkl5*$^{-/-}$) mice, exhibit reduced anxiety with autism-like behaviors.[36–38] Our results show that *Trpc4*$^{-/-}$ mice belong to such a group and that autism-like behavior and anxiolytic behavior might involve a variety of mechanisms in *Trpc4*$^{-/-}$ mice. In addition, *Trpc4*$^{-/-}$ mice exhibited normal levels of motor activity in the OFT. However, their performance in the rotarod test was supra-normal, as reported in several mouse models of ASD.[22] Based on these findings, this increased performance could be interpreted as enhanced performance of a repetitive motor routine.

It is worth noting that Ca^{2+} influx into cortical neurons induced by membrane depolarization leads to a rapid decline in miR-138-2 levels and miR-138 cleavage activity in neurons,[28] and that Ca^{2+} triggers binding of Ca^{2+}/calmodulin (CaM) to MATR3, resulting in impairment of the latter's ability to bind RNAs.[39] In line with this, we observed a prominent increase in MATR3 binding to miR-138-2 in the *Trpc4*$^{-/-}$ mice. This suggests that neuronal activity mediated by TRPC4 may trigger MATR3 binding to Ca^{2+}/CaM, detaching MATR3 from miR-138-2 in the nucleus and increasing cytoplasmic miR-138. Since defects in several ion channels are associated with the pathogenesis of ASD in humans,[6] defects in TRPC4 may be responsible for a specific set of clinical features of ASD. It would be interesting to test whether interfering with the interaction between MATR3 and miR-138-2 would ameliorate those symptoms that are due to TRPC4 deficiency.

Defects in regulation affecting miR-138 signaling appear to underlie some of the core symptoms of ASD in *Trpc4*$^{-/-}$ mice. However, other regulatory factors in addition to MATR3 may be involved in miR-138-2 processing in mature neurons, e.g., Dicer, which binds to the miR-138-2 sequence.[27] Moreover, miR-138 has been shown to indirectly inhibit expression of its own regulator by down-regulating a transcriptional regulator.[40] We found that miR-138 had no such regulatory effect on *Trpc4* mRNA expression. G-protein mediated signaling might also be considered a component of TRPC4-mediated miR-138 processing since G-protein-dependent TRPC4 activation could converge, together with miR-138, on RhoA, which affects spine morphology.[29,41] Inhibition of TRPC4 expression might be linked to a blockade of RhoA activation via APT1-induced palmitoylation of the G-protein.

We found that miR-138-2 was specifically dysregulated in the hippocampus of *Trpc4*$^{-/-}$ mice, where both TRPC4 and miR-138 are normally enriched.[11,16,42,43] This implied that the impact of TRPC4 deletion on miR-138 processing might be strongest in the hippocampus, and we were able to rescue some of the behavioral deficits by hippocampal overexpression of miR-138, suggesting that a lack of hippocampal TRPC4 plays an important role in ASD. This is consistent with the current view that social behaviors involve the hippocampal circuitry.[44] Further, overexpressing miR-138 in the hippocampus partially reversed aspects of the lack of sociability in *Trpc4*$^{-/-}$ mice. It is widely believed that developmental alterations of neuronal networks may be difficult to prevent by pharmacological means after the onset of symptoms.

Therefore, our findings raise the possibility that a single targeted intervention may alleviate multiple behavioral symptoms of autism in mice as late as 8 weeks, the age referred to as 'adult', and long after the onset of pathogenic processes, reinforcing hopes that clinical treatment of ASD could be effective in adult patients. Our results also suggest that restoration of TRPC4 function may benefit a subset of individuals with autism.

Overall, we have been able to demonstrate for the first time that *Trpc4*$^{-/-}$ mice have some of the key symptoms of ASD and that a reduced level of miR-138 may be involved in these symptoms. Given the established role of miR-138 in dendritic spine growth, and the overlap between its synaptic roles and those of other gene products in the neural processes affected in ASD,[28,45] the ability of TRPC4 to regulate miR-138 may provide potential targets for therapeutic interventions in ASD.

Limitations of the study

Our main findings are that TRPC4 might act as a driving force in miR-138-2 processing, determining the levels of miR-138 and thus its targets. Our results indicate that in *Trpc4*$^{-/-}$ mice these processes are oppositely set up, where low miR-138 levels result in upregulation of APT1. This illustrates a potentially disturbing mechanism underlying APT1 expression and spine morphology, including a reduction in mushroom-like spines, in *Trpc4*$^{-/-}$ mice. Our study is limited in that, although ASD is a developmental stage-related disease, we did not compare the importance of TRPC4 across developmental stages. Therefore, further studies are needed to investigate whether TRPC4-mediated neuronal activity induces miR-138-dependent spine signaling, resulting in spine cytoskeletal changes in an age- and activity-specific manner. In addition, it is necessary to study at which developmental stage TRPC4 defects have a significant impact on ASD.

STAR★METHODS

Detailed methods are provided in the online version of this paper and include the following:

- KEY RESOURCES TABLE
- RESOURCE AVAILABILITY
  - Lead contact
  - Material availability
  - Data and code availability
- EXPERIMENTAL MODEL AND SUBJECT DETAILS
  - Mice
- METHOD DETAILS
  - Behavioral studies
  - Repetitive behaviors
  - Three chamber tests
  - Reciprocal social interaction tests
  - Novel object recognition test
  - Open field test
  - Buried food-seeking test
  - Elevated plus maze test
  - Forced swim test
  - Rotarod test
  - Drugs and treatment
  - MiRNA inhibitor treatment
  - Affymetrix whole transcript expression arrays
  - RNA immunoprecipitation
  - Hippocampal dissection
  - Culture of primary hippocampal neurons
  - Quantitative real-Time PCR
  - MiRNA expression analysis by qRT-qPCR
  - Vector construction and virus production
  - Stereotaxic surgery
  - Protein extraction and western blot analysis
  - Immunohistochemistry
  - Dendritic spine analysis
  - Data validation
- QUANTIFICATION AND STATISTICAL ANALYSIS

SUPPLEMENTAL INFORMATION

Supplemental information can be found online at https://doi.org/10.1016/j.isci.2023.108617.

ACKNOWLEDGMENTS

We thank Dr. David E. Clapham (Harvard Medical School, Boston) for providing *Trpc4*$^{+/-}$ mice. This work was supported by the National Research Foundation of Korea (NRF) Grant (2019R1A2C2003616 to H.S.; RS202300240739 to H.S.; 2021R1A2C2011021 to S.J.J.) and the Medical Research Center (MRC) Grant (2017R1A5A2015395) funded by the Ministry of Science and Technology, Republic of Korea (MIST), and the research fund of Hanyang University (HY-202000000700013), Korea.

AUTHOR CONTRIBUTIONS

H.S. defined the research theme, designed the experiments, and wrote the paper. J.Y.S. designed the experiments and conducted the behavioral tests and analysis. H.-R.J., S.H.L., D.G.K., H.L., Y.I.C., Y.L.K., and J.Y.S. carried out the laboratory experiments. J.Y.S. and H.S. analyzed the data and interpreted the results. S.J.J. interpreted the results, provided critical review and discussion, contributed reagents and materials, and wrote the paper. All authors contributed to the interpretation of the results, and J.Y.S. assembled the figures. All authors reviewed and approved the final manuscript.

DECLARATION OF INTERESTS

The authors report no competing interests.

Received: March 7, 2023
Revised: October 8, 2023
Accepted: November 30, 2023
Published: December 2, 2023

REFERENCES

1. Lord, C., Brugha, T.S., Charman, T., Cusack, J., Dumas, G., Frazier, T., Jones, E.J.H., Jones, R.M., Pickles, A., State, M.W., et al. (2020). Autism spectrum disorder. Nat. Rev. Dis. Prim. *6*, 5.
2. Sahin, M., and Sur, M. (2015). Genes, circuits, and precision therapies for autism and related neurodevelopmental disorders. Science *350*.
3. Peça, J., Feliciano, C., Ting, J.T., Wang, W., Wells, M.F., Venkatraman, T.N., Lascola, C.D., Fu, Z., and Feng, G. (2011). Shank3 mutant mice display autistic-like behaviours and striatal dysfunction. Nature *472*, 437–442.
4. Mei, Y., Monteiro, P., Zhou, Y., Kim, J.A., Gao, X., Fu, Z., and Feng, G. (2016). Adult restoration of Shank3 expression rescues selective autistic-like phenotypes. Nature *530*, 481–484.
5. Gandhi, T., and Lee, C.C. (2020). Neural Mechanisms Underlying Repetitive Behaviors in Rodent Models of Autism Spectrum Disorders. Front. Cell. Neurosci. *14*, 592710.
6. da Silva, P.R., do Nascimento Gonzaga, T.K.S., Maia, R.E., and da Silva, B.A. (2022). Ionic Channels as Potential Targets for the Treatment of Autism Spectrum Disorder: A Review. Curr. Neuropharmacol. *20*, 1834–1849.
7. Itsuki, K., Imai, Y., Hase, H., Okamura, Y., Inoue, R., and Mori, M.X. (2014). PLC-mediated PI(4,5)P2 hydrolysis regulates activation and inactivation of TRPC6/7 channels. J. Gen. Physiol. *143*, 183–201.
8. Mori, M.X., Itsuki, K., Hase, H., Sawamura, S., Kurokawa, T., Mori, Y., and Inoue, R. (2015). Dynamics of receptor-operated Ca2+ currents through TRPC channels controlled via the PI(4,5)P2-PLC signaling pathway. Front. Pharmacol. *6*, 22.
9. Griesi-Oliveira, K., Acab, A., Gupta, A.R., Sunaga, D.Y., Chailangkarn, T., Nicol, X., Nunez, Y., Walker, M.F., Murdoch, J.D., Sanders, S.J., et al. (2015). Modeling non-syndromic autism and the impact of TRPC6 disruption in human neurons. Mol. Psychiatr. *20*, 1350–1365.
10. Dulneva, A., Lee, S., Oliver, P.L., Di Gleria, K., Kessler, B.M., Davies, K.E., and Becker, E.B.E. (2015). The mutant Moonwalker TRPC3 channel links calcium signaling to lipid metabolism in the developing cerebellum. Hum. Mol. Genet. *24*, 4114–4125.
11. Fowler, M.A., Sidiropoulou, K., Ozkan, E.D., Phillips, C.W., and Cooper, D.C. (2007). Corticolimbic expression of TRPC4 and TRPC5 channels in the rodent brain. PLoS One *2*, e573.
12. Selvaraj, S., Sun, Y., and Singh, B. (2010). TRPC channels and their implication in neurological diseases. CNS Neurol. Disord.: Drug Targets *9*, 94–104.
13. Bouron, A., Kiselyov, K., and Oberwinkler, J. (2015). Permeation, regulation and control of expression of TRP channels by trace metal ions. Pflügers Archiv *467*, 1143–1164.
14. Riccio, A., Li, Y., Tsvetkov, E., Gapon, S., Yao, G.L., Smith, K.S., Engin, E., Rudolph, U., Bolshakov, V.Y., and Clapham, D.E. (2014). Decreased Anxiety-Like Behavior and G q/11-Dependent Responses in the Amygdala of Mice Lacking TRPC4 Channels. J. Neurosci. *34*, 3653–3667.
15. Lee, S.H., Tonello, R., Choi, Y., Jung, S.J., and Berta, T. (2020). Sensory Neuron–Expressed TRPC4 Is a Target for the Relief of Psoriasiform Itch and Skin Inflammation in Mice. J. Invest. Dermatol. *140*, 2221–2229.e6.
16. Zechel, S., Werner, S., and von Bohlen Und Halbach, O. (2007). Distribution of TRPC4 in developing and adult murine brain. Cell Tissue Res. *328*, 651–656.
17. Meira, T., Leroy, F., Buss, E.W., Oliva, A., Park, J., and Siegelbaum, S.A. (2018). A hippocampal circuit linking dorsal CA2 to ventral CA1 critical for social memory dynamics. Nat. Commun. *9*, 4163.
18. Meyer, M.A.A., Anstötz, M., Ren, L.Y., Fiske, M.P., Guedea, A.L., Grayson, V.S., Schroth, S.L., Cicvaric, A., Nishimori, K., Maccaferri, G., Radulovic, J., et al. (2020). Stress-related memories disrupt sociability and associated patterning of hippocampal activity: a role of hilar oxytocin receptor-positive interneurons. Transl. Psychiatry *10*, 428.
19. Petković, A., and Chaudhury, D. (2022). Encore: Behavioural animal models of stress, depression and mood disorders. Front. Behav. Neurosci. *16*, 931964.
20. Yang, L.P., Jiang, F.J., Wu, G.S., Deng, K., Wen, M., Zhou, X., Hong, X., Zhu, M.X., and Luo, H.R. (2015). Acute Treatment with a Novel TRPC4/C5 Channel Inhibitor Produces Antidepressant and Anxiolytic-Like Effects in Mice. PLoS One *10*, e0136255.
21. Silverman, J.L., Tolu, S.S., Barkan, C.L., and Crawley, J.N. (2010). Repetitive Self-Grooming Behavior in the BTBR Mouse Model of Autism is Blocked by the mGluR5 Antagonist MPEP. Neuropsychopharmacology *35*, 976–989.
22. Rothwell, P.E., Fuccillo, M.V., Maxeiner, S., Hayton, S.J., Gokce, O., Lim, B.K., Fowler, S.C., Malenka, R.C., and Südhof, T.C. (2014). Autism-Associated Neuroligin-3 Mutations Commonly Impair Striatal Circuits to Boost Repetitive Behaviors. Cell *158*, 198–212.
23. Wu, D., Huang, W., Richardson, P.M., Priestley, J.V., and Liu, M. (2008). TRPC4 in Rat Dorsal Root Ganglion Neurons Is Increased after Nerve Injury and Is Necessary for Neurite Outgrowth. J. Biol. Chem. *283*, 416–426.
24. Dictenberg, J.B., Swanger, S.A., Antar, L.N., Singer, R.H., and Bassell, G.J. (2008). A Direct Role for FMRP in Activity-Dependent Dendritic mRNA Transport Links Filopodial-Spine Morphogenesis to Fragile X Syndrome. Dev. Cell *14*, 926–939.
25. Rudy, J.W., and Sutherland, R.J. (1995). Configural association theory and the hippocampal formation: an appraisal and reconfiguration. Hippocampus *5*, 375–389.
26. Banker, S.M., Gu, X., Schiller, D., and Foss-Feig, J.H. (2021). Hippocampal contributions to social and cognitive deficits in autism

spectrum disorder. Trends Neurosci. *44*, 793–807.
27. Weiss, K., Treiber, T., Meister, G., and Schratt, G. (2019). The nuclear matrix protein Matr3 regulates processing of the synaptic microRNA-138-5p. Neurobiol. Learn. Mem. *159*, 36–45.
28. Siegel, G., Obernosterer, G., Fiore, R., Oehmen, M., Bicker, S., Christensen, M., Khudayberdiev, S., Leuschner, P.F., Busch, C.J.L., Kane, C., et al. (2009). A functional screen implicates microRNA-138-dependent regulation of the depalmitoylation enzyme APT1 in dendritic spine morphogenesis. Nat. Cell Biol. *11*, 705–716.
29. Zhu, Y., Lu, Y., Qu, C., Miller, M., Tian, J., Thakur, D.P., Zhu, J., Deng, Z., Hu, X., Wu, M., et al. (2015). Identification and optimization of 2-aminobenzimidazole derivatives as novel inhibitors of TRPC4 and TRPC5 channels. Br. J. Pharmacol. *172*, 3495–3509.
30. Li, H., Mao, S., Wang, H., Zen, K., Zhang, C., and Li, L. (2014). MicroRNA-29a modulates axon branching by targeting doublecortin in primary neurons. Protein Cell *5*, 160–169.
31. Diagnostic and Statistical Manual of Mental Disorders: DSM-5™, 5th ed. (2013 (American Psychiatric Publishing, Inc.).
32. Pobbe, R.L.H., Defensor, E.B., Pearson, B.L., Bolivar, V.J., Blanchard, D.C., and Blanchard, R.J. (2011). General and social anxiety in the BTBR T+ tf/J mouse strain. Behav. Brain Res. *216*, 446–451.
33. Puram, S.V., Riccio, A., Koirala, S., Ikeuchi, Y., Kim, A.H., Corfas, G., and Bonni, A. (2011). A TRPC5-regulated calcium signaling pathway controls dendrite patterning in the mammalian brain. Genes Dev. *25*, 2659–2673.
34. He, Z., Jia, C., Feng, S., Zhou, K., Tai, Y., Bai, X., and Wang, Y. (2012). TRPC5 channel is the mediator of neurotrophin-3 in regulating dendritic growth via CaMKIIalpha in rat hippocampal neurons. J. Neurosci. *32*, 9383–9395.
35. Just, S., Chenard, B.L., Ceci, A., Strassmaier, T., Chong, J.A., Blair, N.T., Gallaschun, R.J., Del Camino, D., Cantin, S., D'Amours, M., et al. (2018). Treatment with HC-070, a potent inhibitor of TRPC4 and TRPC5, leads to anxiolytic and antidepressant effects in mice. PLoS One *13*, e0191225.
36. Kang, M.S., Choi, T.Y., Ryu, H.G., Lee, D., Lee, S.H., Choi, S.Y., and Kim, K.T. (2017). Autism-like behavior caused by deletion of vaccinia-related kinase 3 is improved by TrkB stimulation. J. Exp. Med. *214*, 2947–2966.
37. Chahrour, M., and Zoghbi, H.Y. (2007). The Story of Rett Syndrome: From Clinic to Neurobiology. Neuron *56*, 422–437.
38. Wang, I.T.J., Allen, M., Goffin, D., Zhu, X., Fairless, A.H., Brodkin, E.S., Siegel, S.J., Marsh, E.D., Blendy, J.A., and Zhou, Z. (2012). Loss of CDKL5 disrupts kinome profile and event-related potentials leading to autistic-like phenotypes in mice. Proc. Natl. Acad. Sci. USA *109*, 21516–21521.
39. Malik, A.M., Wu, J.J., Gillies, C.A., Doctrove, Q.A., Li, X., Huang, H., Tank, E.H.M., Shakkottai, V.G., and Barmada, S. (2023). Neuronal activity regulates Matrin 3 abundance and function in a calcium-dependent manner through calpain-mediated cleavage and calmodulin binding. Proc. Natl. Acad. Sci. USA *120*. e2206217120.
40. Hong, Z., Chen, K.H., DasGupta, A., Potus, F., Dunham-Snary, K., Bonnet, S., Tian, L., Fu, J., Breuils-Bonnet, S., Provencher, S., et al. (2017). MicroRNA-138 and MicroRNA-25 Down-regulate Mitochondrial Calcium Uniporter, Causing the Pulmonary Arterial Hypertension Cancer Phenotype. Am. J. Respir. Crit. Care Med. *195*, 515–529.
41. Jiang, L., Liu, X., Kolokythas, A., Yu, J., Wang, A., Heidbreder, C.E., Shi, F., and Zhou, X. (2010). Downregulation of the Rho GTPase signaling pathway is involved in the microRNA-138-mediated inhibition of cell migration and invasion in tongue squamous cell carcinoma. Int. J. Cancer *127*, 505–512.
42. Freichel, M., Vennekens, R., Olausson, J., Stolz, S., Philipp, S.E., Weissgerber, P., and Flockerzi, V. (2005). Functional role of TRPC proteins in native systems: implications from knockout and knock-down studies. J. Physiol. *567*, 59–66.
43. Daswani, R., Gilardi, C., Soutschek, M., Nanda, P., Weiss, K., Bicker, S., Fiore, R., Dieterich, C., Germain, P.L., Winterer, J., and Schratt, G. (2022). MicroRNA-138 controls hippocampal interneuron function and short-term memory in mice. Elife *11*, e74056.
44. Genon, S., Bernhardt, B.C., La Joie, R., Amunts, K., and Eickhoff, S.B. (2021). The many dimensions of human hippocampal organization and (dys)function. Trends Neurosci. *44*, 977–989.
45. Rylaarsdam, L., and Guemez-Gamboa, A. (2019). Genetic Causes and Modifiers of Autism Spectrum Disorder. Front. Cell. Neurosci. *13*, 385.
46. Wang, Y., Zeng, C., Li, J., Zhou, Z., Ju, X., Xia, S., Li, Y., Liu, A., Teng, H., Zhang, K., et al. (2018). PAK2 Haploinsufficiency Results in Synaptic Cytoskeleton Impairment and Autism-Related Behavior. Cell Rep. *24*, 2029–2041.
47. Yang, M., Silverman, J.L., and Crawley, J.N. (2011). Automated three-chambered social approach task for mice. Curr Protoc Neurosci *Chapter*. Curr. Protoc. Neurosci. *Chapter 8*. Unit 8.26.
48. Liu, D., Nanclares, C., Simbriger, K., Fang, K., Lorsung, E., Le, N., Amorim, I.S., Chalkiadaki, K., Pathak, S.S., Li, J., et al. (2022). Autistic-like behavior and cerebellar dysfunction in Bmal1 mutant mice ameliorated by mTORC1 inhibition. Preprint at Mol. Psychiatr.
49. Leger, M., Quiedeville, A., Bouet, V., Haelewyn, B., Boulouard, M., Schumann-Bard, P., and Freret, T. (2013). Object recognition test in mice. Nat. Protoc. *8*, 2531–2537.
50. Machado, C.F., Reis-Silva, T.M., Lyra, C.S., Felicio, L.F., and Malnic, B. (2018). Buried Food-seeking Test for the Assessment of Olfactory Detection in Mice. Bio. Protoc. *8*, e2897.
51. Kim, J.W., Ko, M.J., Gonzales, E.L., Kang, R.J., Kim, D.G., Kim, Y., Seung, H., Oh, H.A., Eun, P.H., and Shin, C.Y. (2018). Social support rescues acute stress-induced cognitive impairments by modulating ERK1/2 phosphorylation in adolescent mice. Sci. Rep. *8*, 12003.
52. Lee, S.H., Kim, N.S., Choi, M., Ko, S.Y., Wang, S.E., Jo, H.R., Seo, J.Y., Kim, Y.S., Kim, H.J., Lee, H.Y., et al. (2021). LGI1 governs neuritin-mediated resilience to chronic stress. Neurobiol. Stress *15*, 100373.
53. Hisaoka, T., Komori, T., Kitamura, T., and Morikawa, Y. (2018). Abnormal behaviours relevant to neurodevelopmental disorders in Kirrel3-knockout mice. Sci. Rep. *8*, 1408.
54. Obernosterer, G., Leuschner, P.J.F., Alenius, M., and Martinez, J. (2006). Post-transcriptional regulation of microRNA expression. RNA *12*, 1161–1167.
55. Hyman, S.L., Levy, S.E., and Myers, S.M.; Council On Children With Disabilities, S.O.D., and Behavioral, P. (2020). Identification, Evaluation, and Management of Children With Autism Spectrum Disorder. Pediatrics *145*.
56. Ko, S.Y., Wang, S.E., Lee, H.K., Jo, S., Han, J., Lee, S.H., Choi, M., Jo, H.R., Seo, J.Y., Jung, S.J., and Son, H. (2019). Transient receptor potential melastatin 2 governs stress-induced depressive-like behaviors. Proc. Natl. Acad. Sci. USA *116*, 1770–1775.
57. Eltokhi, A., Kurpiers, B., and Pitzer, C. (2020). Behavioral tests assessing neuropsychiatric phenotypes in adolescent mice reveal strain- and sex-specific effects. Sci. Rep. *10*, 11263.
58. Honda, T., Yamamoto, Y., Daito, T., Matsumoto, Y., Makino, A., and Tomonaga, K. (2016). Long-term expression of miRNA for RNA interference using a novel vector system based on a negative-strand RNA virus. Sci. Rep. *6*, 26154.
59. Cho, Y., Sloutsky, R., Naegle, K., and Cavalli, V. (2013). Injury-Induced HDAC5 Nuclear Export Is Essential for Axon Regeneration. Cell *155*, 894–908.

STAR★METHODS

KEY RESOURCES TABLE

REAGENT or RESOURCE	SOURCE	IDENTIFIER
Antibodies		
Rabbit anti-APT1 (Lypla1)	Novus Biologicals	Cat# NBP2-17191
Mouse anti-Ephrin B3 (EphB3)	Santa Cruz	Cat# sc271328; RRID: AB_10608991
Rabbit anti-PSD95	Cell signaling	Cat# 2507; RRID: AB_561221
Rabbit anti-Syn1(synapsin1)	Cell signaling	Cat# 5297; RRID: AB_2616578
Conjugated Alexa488	Jackson Immunoresearch	Cat# 016540084; RRID: AB_2337249
Mouse anti-GAPDH	Santa Cruz	Cat# sc25778; RRID: AB_10167668
Rabbit anti-GFP	Thermo Fisher	Cat# a11122; RRID: AB_2307355
Rabbit anti-Lamin B1	Abcam	Cat# ab16048; RRID: AB_443298
Rabbit anti-MATR3	Abcam	Cat# ab70336; RRID: AB_1269374
Mouse anti-βactin	Santa Cruz	Cat# sc47778; RRID: AB_626632
secondary anti-mouse	Jackson ImmunoResearch	Cat# 115-035-003; RRID: AB_10015289
Secondary anti-rabbit	Jackson ImmunoResearch	Cat# 111-035-003; RRID: AB_231356
Chemicals, peptides, and recombinant proteins		
Lipofectamine 2000	Invitrogen	Cat# 11668019
Lipofectamine RNAiMAX Transfection Reagent™	Invitrogen	Cat# 13778075
SensiFASTTM SYBR No-ROX	Bioline	Cat# BIO-98005
Paraformaldehyde	Sigma Aldrich	Cat# 157127
Gibco Neurobasal media	Thermo Fisher	Cat# A2477501
DMEM	Welgene	Cat# LM001-01
Gibco Opti-MEM	Thermo Fisher	Cat# 31985070
Gibco B-27 Supplement, serum free	Thermo Fisher	Cat# 17504044
20X PBS Buffer	Biosesang	Cat# PR2007-100-00
Gibco HBSS (10X)	Thermo Fisher	Cat# 14065-056
Cell lysis buffer (10X)	Cell signaling	Cat# 9803S
1M Tris-HCl	Bioneer	Cat# C-9006
Protease inhibitor cocktail	Sigma Aldrich	Cat# P8340
Phosphatase inhibitor cocktail 2	Sigma Aldrich	Cat# P5726
Phosphatase inhibitor cocktail 3	Sigma Aldrich	Cat# P0044
Protein A-Agarose	Sigma Aldrich	Cat# 11134515001
RNaseOUT™	Invitrogen	Cat# 10777-019
Trypsin EDTA	Welgene	Cat# LS 015-10
Bovine serum albumin	Sigma Aldrich	Cat# A7906
Fetal bovine serum	JRS	Cat# 43640
Gibco Normal goat serum	Thermo Fisher	Cat# 16210072
Penicillin/streptomycin	Welgene	Cat# LS202-02
Glycerol	Sigma Aldrich	Cat# G7757
1M HEPES	Welgene	Cat# BB001-01
HEPES	Sigma Aldrich	Cat# 3375
PEG solution	Sigma Aldrich	Cat# P5413
Phenol red	Sigma Aldrich	Cat# P0290
Trizol reagent	Thermo Fisher	Cat# 15596018

(*Continued on next page*)

Continued

REAGENT or RESOURCE	SOURCE	IDENTIFIER
Sucrose	Sigma Aldrich	Cat# S9378
ImProm-II™ Reverse Transcriptase	Promega	Cat# A3803
Chemicals, peptides, and recombinant proteins		
M084 hydrochloride	TOCRIS	Cat# 1992047-63-8
miRCURY LNA miRNA inhibitor	QIAGEN	Cat# YI04102106-AFA
miRCURY LNA miRNA inhibitor control	QIAGEN	Cat# YI00199006-AFA
Critical commercial assays		
TaqMan™ MicroRNA Reverse Transcription Kit	Thermo Fisher	Cat# 4366596
TaqMan™ Universal Master Mix II, no UNG	Thermo Fisher	Cat# 4440043
Critical commercial assays		
Microarray	Macrogen (Seoul, Republic of Korea)	N/A
Deposited data		
Raw and analyzed data	This paper	Table S1–S4; GEO: GSE220926 https://www.ncbi.nlm.nih.gov/geo/query/acc.cgi?acc=GSE220926
Experimental models: Cell lines		
HEK293T	ATCC	https://www.atcc.org/
Experimental models: Organisms/strains		
C57BL/6J (M. musculus)	The Jackson Laboratory	RRID: IMSR_JAX:000664
Trpc4$^{+/-}$ of 129/SvJ1	Riccio, A et al.[14]	https://doi.org/10.1523/jneurosci.2274-13.2014
HEK293T	ATCC	https://www.atcc.org/; RRID: CVCL_0063
Primary mouse hippocampal neuron cell	This paper	N/A
Oligonucleotides		
Primers for *Trpc4* For: CCGTCTTCTCCGTGTGCTAC Rev: ATGGTTGGTGGTGGACCTTG	This study	N/A
Primers for *Gapdh* For: CTTTGGTATCGTGGAAGGACT Rev: CTTTGGTATCGTGGAAGGACTC	This study	N/A
Primers for Pre-miR-138-2 For: TGC AGCTGGTGTTGTGAATCA Rev: GTGAAATAGCCGGGTAAGAGGAT	This study	N/A
Primers for *MiR-138*	Thermo Fisher	Cat# 002284
Primers for *U6*	Thermo Fisher	Cat# 001973
Chemicals, peptides, and recombinant proteins		
pLenti-III-mir-GFP	Abm	Cat# m001
LentimiRa-GFP-mmu-miR-138-5p	Abm	Cat# mm10073
psPAX2	Addgene	Cat# 12260
pMD2.G	Addgene	Cat# 12259
Software and algorithms		
GraphPad Prism	GraphPad	https://www.graphpad.com/
STELLARIS 8 STED	Leica	https://www.leica-store.co.kr
CFX Manager Software	Bio-Rad Laboratories	https://www.bio-rad.com/
Video camera	Logitech	https://www.logitech.com/
ANY-maze video system	Stoelting Co.	https://stoeltingco.com/
Rotarod apparatus	UGO Basile	https://ugobasile.com
Image J	NIH	https://imagej.nih.gov/ij/

RESOURCE AVAILABILITY

Lead contact

Further information and requests for resources and reagents should be directed to and will be fulfilled by the lead contact, Hyeon Son (hyeonson@hanyang.ac.kr).

Material availability

This study did not generate new unique reagents.

Data and code availability

- The microarray data generated in this publication have been deposited in NCBI's gene Expression Omnibus and publicly available as of the data of publication. Accession numbers are listed in the key resources table.
- This paper does not report original code.
- Any additional information required to reanalyze the data reported in this paper is available from the lead contact upon request.

EXPERIMENTAL MODEL AND SUBJECT DETAILS

Mice

All experiments were conducted with 2-8-week-old male C57BL/6 mice (Koatech, Pyeongtaek, Korea) and *Trpc4*$^{-/-}$ male mice. Heterozygous littermates (*Trpc4*$^{+/-}$) of 129/SvJ1 mice were generously provided by Professor Clapham.[14] TRPC4 heterozygotes (*Trpc4*$^{+/-}$) were back-crossed with a C57BL/6J inbred background over 10 generations, and heterozygous breeders were crossed to generate wild-type (*Trpc4*$^{+/+}$), heterozygous (*Trpc4*$^{+/-}$), and *Trpc4*$^{-/-}$ littermates. Behavioral experiments were performed with 8-12-week-old male *Trpc4*$^{-/-}$ mice, and age-matched male wild-type littermates were used in each experiment. Animals were maintained under a 12-h light/dark cycle with food and water *ad libitum*. Animal protocols were approved by the Institutional Animal Care and Use Committee of Hanyang University.

METHOD DETAILS

Behavioral studies

Before beginning each of the behavioral tests, the mice were placed in the testing room for 1 h and acclimated to room conditions. All tests were conducted during the dark housing cycle and in random order. After each test session, the apparatus was cleaned with 70% alcohol to remove any odor and trace of the previously tested mouse. The experimenter running the tests was blind to mice group.

Repetitive behaviors

The repetitive behavior test was performed in the home cage.[46] Grooming behavior was video-recorded for 20 min. Time spent on grooming behavior such as scratching the face, head, or back with either forelimb, and rearing behavior was measured. Repetitive behavior was measured by an observer who remained blind to mouse genotype.

Three chamber tests

To investigate sociability (tendency to social contact with a stranger mouse versus an inanimate object) and social novelty preference (tendency to social contact with a novel stranger versus a familiar mouse), we used the three-chambered social approach test.[36] The three-chamber apparatus was a transparent white plastic box with two transparent acrylic partitions with a square opening (10 × 10 cm). The acrylic partitions divided the box into three chambers (left, center, and right; 20 × 45 cm each). Each side-chamber contained a cylindrical wire cage (8.5 cm) in the corner to hold a stimulus mouse. A cylindrical bottle filled with water was placed on top of the wire cup to prevent the mouse from climbing over the cup. All stranger mice were age-matched male C57BL/6 mice, which were acclimated to the wire cages for 10 min before beginning the test. The test consisted of three phases: habituation, sociability, and social novelty preference. In phase 1, the test mouse was placed in the central chamber for 10 minutes and allowed to explore the 3 chambers. In phase 2 (sociability), two identical cages (cup-shape with evenly spaced metallic bars of diameter 8.5 cm) were placed into the left and right chambers, respectively, and a stranger mouse of the same sex, and similar age and size to the testing mouse was put inside the left cage. The testing mouse was allowed to explore the 3 chambers for 10 minutes. In phase 3 (social novelty recognition), the procedure was the same as in stage 2 except that a stranger mouse of the same sex, similar age and size as the testing mouse occupied the right cage. Approach behavior by the targets was defined as interaction in terms of sniffing time. All stages were video-recorded. Exploration time in each chamber was analyzed by the ANY-maze tracking system (Stoelting Co., IL, USA). Sniffing was defined when the subject mouse was close to the cup and its nose was oriented to the cup.[47] Times for the test mouse to face and sniff the novel mouse-containing cage and the empty cage were measured by an observer who remained blind to mouse genotype. Times spent in close interaction with each wire cage were converted into preference index. The sociality index was calculated as ([T-mouse − T-empty]/[T-mouse + T-empty]) x 100. The preference index in the social novelty preference test was calculated as: ([time spent exploring the stranger mouse] − [time spent exploring the familiar mouse])/[total time spent exploring both targets] × 100.

Reciprocal social interaction tests

For the reciprocal social interaction test,[48] mice were placed in the corner of an open area (50 × 50 × 20 cm) and an adult male test mouse was placed in the opposite corner. Behavior was recorded using a video camera located above for 5 min. Time spent in physical contact was analyzed using a stopwatch. Numbers and durations of active contact (i.e., test mouse contacting the WT mouse), the numbers of followings, of nose-to-anogenital sniffs, and of nose-to-nose sniffs, and those of physical contact (including both active and passive contacts) were analyzed manually by an observer who remained blind to genotype.

Novel object recognition test

A mouse was allowed to explore the box for 5 min on the day before the test,[49] and returned to the home cage. The next day, it was placed in an open area, its head positioned opposite the objects. A stopwatch as used to measure the time needed to reach the 20 s criterion of total exploration and a second stopwatch recorded the time spent exploring each object. The second stopwatch was equipped with two channels to record exploration times for each object. The next day, the two familiar objects were replaced, one with an object like the previous one and the other with a novel object. They were placed at the same location, 5 cm away from the walls. Each mouse was observed for 10 min.

Open field test

Mice were placed in a corner of a white plastic box (50 × 50 × 20 cm) to initiate the test session, and their movements were recorded for 30 min with a web camera (HD C310, Logitech, Switzerland) fixed over the apparatus. Total locomotor activity was measured using an ANY-maze video tracking system (Stoelting Co., IL, USA).

Buried food-seeking test

For the buried food-seeking test,[50] mice were food-deprived for 24 hrs before the test. A 2 g pellet of regular chow was buried 8 cm beneath the surface of fresh bedding in a corner of the test cage. Mice were placed in the test cage in the corner opposite the buried pellet and the time to find the food pellet was monitored. The mice were stopped as soon as they found the pellet, within a maximum 10 min period, and the latency was recorded.

Elevated plus maze test

The elevated plus-maze apparatus consisted of two closed arms (30 x 8 cm) and two open arms (30 x 8 cm).[51] Mice were placed in the center (8 x 8 cm) to initiate the test. The apparatus was placed 50 cm above floor level in the light. In the EPM test, mice were individually placed in the central area and allowed to move freely for 6 min. Each mouse was recorded using an ANY-maze video tracking system (Stoelting Co., IL, USA). The percentage of time spent in the open arms, the number of entries to the open arms, and the total distance traveled were measured.

Forced swim test

Mice were placed individually in a transparent plastic cylinder (30 cm high, 15 cm in diameter) containing water at 24 $\pm$ 1°C and a depth of 15 cm, and were forced to swim for 6 min. Their behavior was recorded with a video camera (HDR-PJ230, Sony, Japan). Immobility time was scored manually during the 6 min.[52]

Rotarod test

Motor coordination and motor learning were assessed using an accelerating rotarod apparatus (UGO Basile, VA, Italy) as described previously[53] with some modifications. Each test mouse was placed on a rotating drum (3 cm diameter) for a maximum of 5 min, and the latency to fall from the rotating drum was measured. The speed of the rotating drum increased from 4 to 44 rpm over a 5-min period. Mice were given three training trials (trainings 1–3) with intertrial intervals of 30 min on the first day and one test trial on the second day. Each trial was terminated when a mouse fell off, made one complete backward revolution while hanging on, or after 300 s (maximum speed, no further acceleration). During a trial, mice that turned 180 to face backward (the same direction as rotation) were gently guided to turn around and face forward (the opposite direction of rotation).

Drugs and treatment

M084 (TOCRIS, Bristol, UK), was dissolved in water. Animals received intraperitoneal (i.p) injections of vehicle or M084 (at 20 mg/kg body weight) 2 hrs before the behavioral tests.[54] The dose of M084 given was based on the IC_{50} of M084 (3.7-10.3 μM) for the TRPC4β channel by various assays.[20]

MiRNA inhibitor treatment

The procedure used for inhibition was as described previously.[28] Primary hippocampal neuron cell transfection was performed by the lipofectamine RNAiMax transfection reagent (Invitrogen, CA, USA) according to the manufacturer's instructions. One day before the transfection was performed, the primary cell was changed in the neurobasal (NB) medium without 1% 100X penicillin/streptomycin antibiotic (P/S). On the 13th day of differentiation (DIV 13), 50 nM of the control miRNA or anti-miR-138-5 (Qiagen, Maryland, USA; miRCURY LNA™ miRNA negative

control and miRNA inhibitor, dissolved in TE buffer) were mixed with 4.5 μl lipofectamine RNAiMax Transfection Reagent™ in 50 ul NB medium without P/S. Then, the mixed complex was incubated for 15 min at room temperature and added to the cells. The next day, primary cells were changed to NB medium, including B27, P/S, and L-glutamate, and the medium was replaced every other day. On DIV18, proteins and RNA were isolated to investigate the inhibitory effect of miR-138.

Affymetrix whole transcript expression arrays

The Affymetrix Whole Transcript Expression arrays were used according to the manufacturer's protocol (GeneChip Whole Transcript PLUS reagent Kit). RNA purity and integrity were evaluated with an ND-1000 spectrophotometer (NanoDrop, Wilmington, USA), and Agilent 2100 Bioanalyzer (Agilent Technologies, Palo Alto, USA). cDNA was synthesized using a GeneChip WT (Whole Transcript) Amplification kit as described by the manufacturer. The sense cDNA was then fragmented and biotin-labeled with TdT (terminal deoxynucleotidyl transferase) using a GeneChip WT Terminal labeling kit. Approximately 5.5 μg of labeled DNA target was hybridized to the Affymetrix GeneChip Mouse 2.0 Array (Affymetrix, Santa Clara, CA) containing 698,000 unique 25-mer oligonucleotides constituting over 33,000 gene-level probe sets at 45°C for 16 h. Hybridized arrays were washed and stained on a GeneChip Fluidics Station 450 and scanned on a GCS3000 Scanner (Affymetrix). Signal values were computed using Affymetrix® GeneChip™ Command Console software. The data were summarized and normalized with the robust multi-average (RMA) method implemented in Affymetrix® Power Tools (APT). We exported the results with gene-level RMA analysis and performed a differentially expressed gene (DEG) analysis. Statistical significance of the expression data was determined using the LPE test and fold changes, the null hypothesis being that no difference existed between groups. The false discovery rate (FDR) was controlled by adjusting the *P*-value using the Benjamini-Hochberg algorithm. For the DEG set, we employed hierarchical cluster analysis using complete linkage and Euclidean distance as a measure of similarity. Gene-Enrichment and Functional Annotation analysis for the significant probes was performed using Gene Ontology (www.geneontology.org/) and KEGG (www.genome.jp/kegg/). All data analysis and visualizations of the DEG were conducted using R 3.3.2 (www.r-project.org). The genome-wide microarray analysis is reported in Tables S1–S4.

RNA immunoprecipitation

Hippocampi were homogenized in lysis buffer (Cell signaling, MA, USA) containing protease inhibitor, phosphatase inhibitors II and III, and RNase OUT (Invitrogen). Lysates (1-3 mg) were immunoprecipitated with 20-35 μg antibody (MATR3, Abcam, ab70336) or rabbit IgG (Millipore, CA, USA) in HNTG buffer (20 mM HEPES pH 7.5, 150 mM NaCl, 0.1% Triton X-100 and 10% glycerol) containing protease, phosphatase inhibitors, and RNase OUT at 4°C overnight. Antibody was added at 4°C for 2 h followed by immunoprecipitation with 100 μl of protein A-agarose beads (Roche, Mannheim, Germany) and three washes with the same HNTG buffer. The bound proteins were incubated at 55°C for 30 min in RIP buffer (50 mM Tris-HCl pH 8.0, 1 mM EDTA, 1% SDS) including proteinase K (Roche) and RNA was extracted. In RNA-binding protein immunoprecipitation (RIP) data analysis, the cycle threshold[55] value of each RIP RNA fraction was normalized to the C_t value of the input RNA fraction in the same quantitative PCR Assay (ΔC_t) to account for RNA sample preparation differences. Then, the normalized RIP fraction C_t value (ΔC_t) was adjusted for the normalized background (anti-IgG) [nonspecific Ab] fraction C_t value ($\Delta\Delta C_t$). The fold enrichment [RIP/nonspecific] was calculated by linear conversion of the $\Delta\Delta C_t$. Shown below are the formulas used for the calculation: ΔC_t [normalized RIP] = (C_t [RIP] – (C_t [Input] – Log_2 (Input/IP Dilution Factor)); $\Delta\Delta C_t$ [RIP/nonspecific] = ΔC_t [normalized RIP] – ΔC_t [normalized nonspecific]; fold enrichment = $2^{-\Delta\Delta Ct\left[\frac{RIP}{nonspecific}\right]}$.

Hippocampal dissection

Mice were killed by cervical dislocation. The brain was removed and chilled in ice-cold 1X HBSS, and all further manipulations were performed on an ice-cooled plate. The whole of the hippocampus was dissected from the brain, and 500 μm-thick transverse slices were cut with a Starrett tissue chopper. The dentate gyrus (DG) was micro-dissected by hand under a dissecting microscope. Subregional boundaries were visible under these conditions. Tissues were collected and stored at −80°C.

Culture of primary hippocampal neurons

Whole brains were collected from C57BL/6 mouse E14 embryos.[56] The embryonic hippocampus was dissected in ice-cold Ca^{2+}/Mg^{2+}-free HBSS (Gibco), followed by the removal of blood vessels and meninges. The hippocampal tissue was then incubated with 0.05% trypsin-EDTA (Welgene, Korea) at 37°C for 5–10 min, and dissolved in neurobasal (NB) medium (Gibco) containing 10% (v/v) FBS (Welgene, Korea), 0.5 mM L-glutamine (Sigma, USA), and 1% P/S (Welgene, Korea). After centrifugation at 1500 rpm for 1 min, the pelleted cells were gently resuspended in the culture medium and plated at 60,000 – 80,000 cells per cm^2 on poly-L-lysine-coated (25 μg/mL in PBS; Sigma, USA) and laminin-coated (10 μg/ml in PBS; Invitrogen, CA, USA) culture dishes. Hippocampal cultures were grown for 1 d in NB medium containing 10% (v/v) FBS, 0.5 mM L-glutamine, and 1% P/S. The medium was changed the following day to NB medium supplemented with 2% (v/v) B27 (Gibco) serum-free supplement, 0.5 mM L-glutamine, and 1% 100X P/S mixture. Cultures were maintained for 7–18 d at 37°C in a 5% CO_2 and 95% air-humidified incubator. The neurons were used after 7–18 d.

Quantitative real-Time PCR

Total RNA was isolated from mouse hippocampal tissue using Trizol reagent (Invitrogen, CA, USA).[52] Reverse transcription of 1 μg of total RNA was performed with oligonucleotide deoxythymidine primers using Improm-II TM Reverse Transcription System (Promega, WI, USA). The resulting cDNA was used as template for the amplification of target gene transcripts by real-time PCR. Quantitative real-time PCR (qPCR) was performed on a CFX96 Touch™ Real-Time PCR Detection System (Bio-Rad Laboratories, CA, USA) using SensiFASTTM SYBR No-ROX mix (Bioline). Quantitative real-time PCR (qPCR) was performed on a CFX96 Touch™ Real-Time PCR Detection System (Bio-Rad Laboratories, CA, USA). GAPDH was used to normalize the threshold cycle[57] values, and gene expression was quantified by the relative quantitation method ($2^{-\Delta\Delta Ct}$).[27]

MiRNA expression analysis by qRT-qPCR

miRNAs were reverse transcribed with a TaqMan MicroRNA Reverse Transcription Kit (Applied Biosystems, Foster City, CA, USA).[58] In brief, 10 ng of total RNA was used to synthesize cDNA for miRNAs using MultiScribe™ Reverse Transcriptase and miRNA-specific RT primers (5×) by incubating at 16°C for 30 min, 42°C for 30 min, and 85°C for 5 min. cDNA samples for specific miRNAs were subjected to real-time qPCR. Data were analyzed by the $2^{-\Delta\Delta Ct}$ method with U6 snRNA as housekeeping control for normalization.

Vector construction and virus production

To reproduce increased miR-138 dosage, the miR-138 sequence (MIMAT0000150) was retrieved from miRNA miRBase, and then LentimiRa-GFP-mmu-miR-138-5p (pLenti-miR-138-2) and pLenti-III-miR-GFP control (pLenti-miR-Neg.control) were purchased (Applied Biological Materials Inc., Richmond, Canada). The human embryonic kidney epithelial 293T cells (ATCC) were cultured in DMEM (Invitrogen, CA, USA) supplemented with 10% fetal bovine serum (JRS, 43640) and 1% P/S (Welgene) as growth medium. 293T cells were transfected using the lipofectamine 2000. 3×10^6 cells of 293T were seeded in the 100-mm dish at 60∼70% confluence the day before transfection. One day before the transfection was performed, 293T cells were changed in the Opti-MEM medium. To produce the virus, 12 μg of lentiviral LentimiRa-GFP-mmu-miR-138-5p or empty pLenti-III-miR-GFP control vector were transiently co-transfected with the compatible packaging plasmids, 8 μg psPAX2 and 6 μg pMD2.G into 293T cells using lipofectamine 2000. After 12 h, the medium was changed to DMEM growth medium supplemented with 20% BSA (Sigma, USA) and 1 M HEPES (Sigma, USA). After 48 h posttransfection, the medium was collected, centrifuged at 1,500 rpm 4°C for 5 min to remove cell debris, and sterilized using 0.45 μm low protein binding syringe filters (ADVANTEC). For virus concentration, the collected lentiviral supernatant was added to a 5X PEG solution (Sigma, USA) and incubated overnight at 4°C. The next day, the mixture was centrifuged at 3,000 rpm 4°C for 30 min and the pellet was incubated with 1X PBS containing 1% BSA on the shaker at 4°C. The produced viruses were collected and stored at −80°C.[52]

Stereotaxic surgery

Mice were anesthetized with a mixture of Rompun (8.5 mg/kg) and Zoletil (17 mg/kg), and prepared for stereotaxic surgery. Lentiviral preparations were delivered to coordinates based on the Franklin and Paxinos atlas to the DR: ML ±0.15 mm; AP -0.2 mm; DV -0.24 mm. lentivirus (1-2 μl) was injected bilaterally into each DG of the dorsal hippocampus using a Hamilton syringe (26G) at a rate of 0.15 μl/min.

Protein extraction and western blot analysis

Protein extract from hippocampal tissue or cultured hippocampal neurons was subjected to SDS-PAGE, transferred to PVDF membrane, and incubated with antibodies. Extraction of nuclear protein was described previously.[59] Hippocampal tissue was dissected quickly on ice and homogenized in 1X HBSS buffer with HEPES and phenol red. Homogenization was performed manually with 8–10 gentle strokes in a tissue grinder, and the homogenate was centrifuged for 25 min at 13,000 rpm at 4°C. Homogenates were stored at -20°C. For the nuclear and cytosol extraction, Hippocampi were homogenized in ice-cold cytosol extraction buffer (0.5% Triton X-100, 50 mM Tris-HCl, protease inhibitor cocktail [10 μl/ml], and phosphatase inhibitor cocktails [10 μl/ml]). After 10 min on ice, homogenates were centrifuged (13,000 rpm, 20 min, 4°C). The supernatants were saved as the cytoplasmic fraction. Pellets were washed in ice-cold cytosol fraction buffer without protease and phosphatase inhibitors and sedimented by centrifugation at 13,000 rpm for 5 min at 4°C. The supernatant was removed, and nuclei were re-suspended in ice-cold nuclear extraction buffer (50 mM Tris-HCl, 1% Triton X-100, 0.4 M NaCl, protease inhibitor cocktail [10 μl/ml] and phosphatase inhibitor cocktails [10 μl/ml]). Samples were vortexed every 5 min for 30 min. The nuclear fractions were centrifuged at 13,000 rpm, for 20 min at 4°C. The supernatants were stored at -20°C. The protein assay was used for quantitation of total protein in lysates using BSA as a protein standard. (5000002, Bio-Rad, CA, USA). Primary antibodies were diluted in 1X TBS with 0.1% (v/v) Tween-20, as follows: anti- APT1 (1:500, NBP2 17191, Novus), anti-EphB3 (1:1000, sc271328, Santa Cruz), anti-PSD95 (1:2000, #2507, Cell signaling), anti-Syn1 (1:2000, #5297, Cell signaling), anti-MATR3 (1:1000, ab70336, Abcam), anti-βactin (1:2000, sc47778, Santa Cruz), anti-GAPDH (1:1000, sc25778, Santa Cruz), anti- LaminB1 (1:1000, ab16048, Abcam). Secondary antibodies were diluted in 1X TBS with 0.1% (v/v) Tween-20 containing 5% (w/v) non-fat dry milk, as follows: anti-rabbit and anti-mouse IgG conjugated with HRP (1:1000,111-035-003, Jackson ImmunoResearch). Blots were developed with enhanced chemiluminescence western blotting detection system (ECL STAR; Dyne Bio, Korea). Optical density was measured using Image J software to quantify the blots.

Immunohistochemistry

Mice were transcardially perfused with cold 4% paraformaldehyde in PBS for 20 min and processed for histology.[56] Brains were postfixed in the same solution overnight at 4°C and stored in 30% (w/v) sucrose at 4°C. Serial sections (25 μm) were cut coronally through the entire hippocampus and stored in 50% glycerol in PBS at 20°C. To detect green fluorescent protein (GFP), sections were incubated overnight with biotinylated goat anti-GFP antibody (a11122, Thermo Fisher) at pH 7.4, 4°C, containing 0.3% Triton X-100 in PBS (PBST). The next day, the sections were washed three times with 1% NGS and 0.3% Triton X-100 in PBS for 15 min and incubated with streptavidin-conjugated Alexa488 (code 43016480084, Jackson Immunoresearch) secondary antibodies in 1% normal goat serum in PBS for 2 h. Optical sectioning was used during the acquisition of Z-stack images. LAS AF software (Leica Microsystems, Wetzlar, Germany) was used to sharpen images, adjust brightness and contrast levels, and compose Z-projection (maximum intensity) and channel-merged figures. For dendritic analysis, the samples were photographed in the molecular layer of DG.

Dendritic spine analysis

For dendritic analysis, 40 single neuron images from the hippocampus of both genotypes (10 neurons per mouse) were captured in a confocal microscope (Stellaris 8.0 STED, Leica Microsystems, Wetzlar, Germany) coupled to a Hamamatsu Flash 4.0 V3 (Scientifica Ltd., East Sussex, UK). A series of Z-stack images were taken (distance between images: 2 μm) for each neuron by optical sectioning. Z-stack images were uploaded to the LAS AF software to sharpen images, adjust brightness and contrast levels, and compose Z-projection (maximum intensity). A well-stained neuron shows complete dendrite filling and well-stained dendritic spines across the dendritic shafts, with no breaks in dendritic branches, and is isolated from surrounding neurons. In the molecular layer of DG, regions between the first- and second- order branches of the dendrites located at 30- to 200-μm distances from the center of the cell body were traced, and the spines were counted. Totally two dendrites per single neuron were selected from each mouse. The spine densities were averaged across animals in each group.

Data validation

No sample-size calculation was performed, but our sample sizes are similar to those reported in previous publications.[3,36] On average, above 7 animals per group were analyzed for behavioral studies, and above 2 animals per group were analyzed for biochemical experiments. Exact numbers of animals and cells were provided in figure legends. All the data were included, except for those with unsuccessful sampling, such as damaged brain tissue for histology or technical errors in video recording. All biological data represent independently collected replicates unless specifically stated. All attempts at replication were successful, and the biological replicate number corresponds to the number of mice. Technical replicates were not performed in this study. Individual data is presented for transparency. All animals were age and sex matched for all studies, as stated in Methods, and samples were allocated by genotype. For behavioral studies, animals were randomly assigned to different experimental groups, and the order of animals tested was distributed across groups under common experimental conditions. Behavioral studies were carried out by experimenters who were not aware of the animal group allocations. The outcome was assessed blindly by other investigators.

QUANTIFICATION AND STATISTICAL ANALYSIS

Statistical analyses were performed using GraphPad Prism 7.0 software (GraphPad Software, Inc., La Jolla, CA, USA). Unpaired Student's *t* tests were used to compare 2-group data. Two-way ANOVA followed by Newman Kuals was used for multiple comparisons between groups when assessing the effect of genotype and lenti-shRNA infusion on behaviors. Behavioral findings were successfully replicated with mice from different litters and, in several instances, across at least three independent cohorts. Sample sizes for behavioral studies were determined based on similar work in the literature. The detailed statistical information is shown in Tables S5 and S6, respectively. All biochemical experiments were carried out at least three times, and data were consistent in repeated experiments. $p < 0.05$ was considered statistically significant, and all data are presented as means ± SEM.